

# Path length and sediment transport estimation from DEMs of Difference: a signal processing approach

Lindsay Capito<sup>1</sup>, Enrico Pandrin<sup>2</sup>, Walter Bertoldi<sup>2</sup>, Nicola Surian<sup>1</sup>, Simone Bizzi<sup>1</sup>

<sup>1</sup>Department of Geosciences, University of Padova, Padova, 35131, Italy

<sup>2</sup>Department of Civil, Environmental, and Mechanical Engineering, University of Trento, Trento, 38122, Italy

Correspondence to: Lindsay Capito (lindsaymarie.capito@studenti.unipd.it)

**Abstract.** The difficulties of measuring bedload transport in gravel bed rivers have given rise to the morphological method wherein sediment transport is inferred from changes in riverbed elevation and estimates of the distance traveled by sediment, its path length. Because current methods for estimating path length are time and labor intensive, we present a method to estimate a characteristic path length from repeat digital elevation models (DEMs of difference i.e., DoDs). We propose an automated method to extract the spacing between erosional and depositional sites on the DoD by the application of Variational Mode Decomposition (VMD), a signal processing method, to quantify the spacing as a proxy for path length. We developed this method using flume experiments where bed topography and sediment flux were measured and then applied it to published field data with physical path length measured from tracer measurements for validation. Our path length estimates had an error lower than 30% when compared to the measured mode of the tracer distances in the field and generated sediment transport estimates were not significantly different than the measured sediment flux at lower discharges in the lab. However, we observed an underestimation of sediment flux at the higher discharges in the flume study. We explore explanations for the underestimation and we interpret this as a limit of the method in confined settings, where sediment transport becomes decoupled from morphological changes. We also explore how the time between survey acquisitions, the morphological active width relative to the channel width, and DoD thresholding techniques affect the proposed method and the potential issues they pose to the morphological method in general.

## 1 Introduction

In gravel bed rivers sediment transport fundamentally controls morphological processes but is notoriously difficult to measure due to its spatial and temporal heterogeneity (Hoey, 1992; McLean and Church, 1999) measurement uncertainty (Vericat et al., 2006), and the logistical challenges of field measurements. The morphological approach is a method to estimate bedload transport based on observed changes in morphology coupled with an estimate of how far sediment travels, the path length (Ashmore and Church, 1998), or a known flux at one boundary (Grams et al., 2013). With the increasing availability of high resolution topography, it is now easier to quantify the volume of mobilized sediment needed for the morphological method from the comparison of repeat topographic surveys known as digital elevation models (DEMs) whereby the older survey is subtracted from the newer survey to obtain a DEM of difference (DoD). However, the estimation of path length remains a challenge.

Implementation of the path length based approach requires an estimation of typical particle travel distances for the reach in question. Historically, these distances have been estimated using tracers, either electronically tagged or painted clasts. Unfortunately, tracer studies are time and labor intensive, requiring multiple site visits and intensive recovery campaigns which often have low recovery rates, especially for painted clasts (Hassan and Bradley, 2017; Brenna et al., 2019). Furthermore, tracer studies are often applicable only to exposed bars, ignoring a large portion of in-channel transport, and

**Style Definition:** Bibliography: Space After: 12 pt, Line spacing: single

can be sensitive to the seeding location (Liébault et al., 2012). To overcome these limitations, several methods have been proposed to estimate path length based on the connection to morphology.

~~Given that morphological units are the cumulative result of the displacement of sediment particles, it follows that the two would be related. Neill (1971) proposed that path length in meandering rivers should be equal to the distance from an erosional site (eroding bank) to the next depositional site (point bar) downstream. Many others have observed similar relationships based on the spacing of erosional and depositional sites and channel morphology (Beechie, 2001; Hundey and Ashmore, 2009; Kasprak et al., 2015; Pyree and Ashmore, 2003b, a; Vázquez-Tarrío et al., 2019). A synthesis of tracer studies demonstrated that at formative discharges, particle path length distributions often exhibit primary or secondary modes corresponding to the location of bars, where deposition occurs (Pyree and Ashmore, 2003a). Further, depositional areas (typically bars), have demonstrated a higher probability of 'trapping' particles than erosional morphological units (McDowell and Hassan, 2020; McDowell et al., 2021). Finally, experimental research has confirmed the preferential deposition of particles specifically at bar heads and margins even in channels with more complex morphology, for example, in braided rivers (Kasprak et al., 2015) but it is reasonable to assume that in multithreaded channels, multiple path lengths might exist at different flow stages in primary and secondary channels.~~

~~Given the observations linking path length to morphology, we hypothesize that path length can be inferred from changes in morphology at near event scale comparisons. If during a flood, sediment is mobilized from an area of erosion to an area of deposition as represented on the DoD, the distance between the two should correspond to a typical path length. Following this hypothesis, this work has the following objectives: i) to propose an efficient and semiautomatic method to quantify the distance between sites of erosion and deposition from the DoD; ii) to use these estimates of path length to explore the feasibility and accuracy of sediment transport flux estimations, using direct measurements at the laboratory scale; iii) to compare these estimates to measured path lengths obtained from tracer data in the field; iv) and finally to evaluate the potential sources of error when estimating sediment flux from changes in morphology.~~

## ~~2 Methods~~

~~To meet our objectives, we use flume experiments at varying discharges with direct measurement of output sediment flux and sets of repeat DEMs from which DoDs are created and used to identify patterns of erosion and deposition.~~

~~1 Introduction~~  
~~In gravel bed rivers sediment transport fundamentally controls morphological processes but is notoriously difficult to measure due to its spatial and temporal heterogeneity (Hoey, 1992; McLean and Church, 1999) measurement uncertainty (Vericat et al., 2006), and the logistical challenges of field measurements. We then develop a semiautomated method to extract these distances between erosion and deposition and compare our estimates to measured sediment flux. Finally, we test this method using published field data with tracer measurements as validation of the path length estimates.~~

### ~~2.1 The morphological method~~

Formatted: Normal

The morphological approach is a method to estimate bedload transport based on observed changes in morphology. There have been many implementations of the morphological method since its inception and it has been reviewed extensively (Ashmore and Church, 1998; Brewer and Passmore, 2002; Church, 2006; Vericat et al., 2017). With the increased availability of hydrologic data and modeling capabilities the morphological method has also been applied in two dimensions (x,y) by coupling a 2D hydraulic model to account for sediment routing (Lane et al., 1995; Antoniazza et al., 2019; Bakker et al., 2019). These 2D applications shed light on the functional links between topographic changes and spatial distribution of bedload transport. Antoniazza et al., (2019) quantified the errors in estimating sediment transport with a 1D approach where 2D cross-stream sediment fluxes are neglected which may be especially useful in multithreaded channels. They also explored how DEM accuracy and the frequency of acquisitions affect the estimates of sediment fluxes derived by the morphological method. These contributions confirm the applicability of the morphological method to estimate sediment transport, however, they require intensive field campaigns and an accurate accounting of upstream water and sediment supplies, often not available in real case studies. In this paper the desire is to explore novel approaches to apply the morphological method using topographic data alone, as hydraulic and sediment supply data are not available in many applications and management situations.

The morphological method can be formalized based on the sediment continuity equation:-

$$(Q_{bin} - Q_{bout})\Delta t = (1 - p)\Delta V \quad (1)$$

Where  $Q_{bin}$  and  $Q_{bout}$  are the volumetric sediment flux in and out of the reach respectively,  $\Delta t$  is the time between surveys,  $p$  is the sediment porosity, and  $\Delta V$  is the change in volume. The sediment continuity equation can be solved in several ways, ~~one~~ but in addition to  $\Delta V$  measured from the DoDs, it requires that either the incoming flux  $Q_{bin}$  or the outgoing flux  $Q_{bout}$  be defined. In most cases, neither of these fluxes are known, as they are the exact parameters that need to be estimated when applying the morphological method. This conundrum has been ~~estimated~~ addressed by setting a zero-flux boundary, such as a dam or gravel sand transition (McLean and Church, 1999), by segmenting the reach such that a zero-flux boundary is set between a section of net deposition to one of net erosion (Vericat et al., 2017) or by measuring flux either into or out of the reach (Grams et al., 2013); (Vericat et al., 2017; Calle et al., 2020) or by measuring flux either into or out of the reach (Grams et al., 2013; Antoniazza et al., 2019).

Alternatively, Eq. (1) can be modified so that active layer depth,  $d_s$  and width  $w_s$  and the virtual velocity,  $v_b$  are used:-

$$Q_b = v_b \frac{L}{T} = \frac{L}{T} d_s w_s (1 - p) \rho_s \quad (2)$$

Where  $v_b$  is equal to  $L/T$ ,  $L$  being the distance the particles travel and  $T$  the time over which the particles are traveling (Church, 2006). The virtual velocity approach has been successfully applied using tracer gravels to estimate the path length parameter  $L$  in a variety of morphological settings (Liébault et al., 2012; Mao et al., 2017; Brenna et al., 2019, 2020; Brenna and Surian, 2023). Unfortunately, tracer studies are time and labor intensive, requiring multiple site visits and intensive recovery campaigns which often have low recovery rates, especially for painted clasts (Hassan and Bradley,

Formatted: Left, Indent: Left: 2.5"

2017; Brenna et al., 2019). Furthermore, tracer studies are often applicable only to exposed bars, ignoring a large portion of in-channel transport, and can be sensitive to the seeding location (Liébault et al., 2012). To overcome these limitations, several methods have been proposed to estimate path length based on the connection to morphology.

The term path length describes the distance traveled by a particle from entrainment to deposition during a transport event and is punctuated by shorter bursts of movement termed step lengths (Einstein, 1937). Individual particles do not all entrain, travel, and deposit together in unison but rather form a distribution of path lengths potentially dependent on grain size, flow strength and duration, and channel morphology. The relative strength of these physical controls on path length has been explored with varied results. Some studies have found relationships between path length and flow metrics such as stream power (Hassan et al., 1992; Schneider et al., 2014; Vázquez-Tarrío and Batalla, 2019; Vázquez-Tarrío et al., 2019) but a considerable scatter in the data has reinvigorated the debate over the role of morphology as a primary control of path length (Hassan and Bradley, 2017; Vázquez-Tarrío and Batalla, 2019; Vázquez-Tarrío et al., 2019).

The connection between morphology and path length has long been discussed. Neill (1971) proposed that path length in meandering rivers should be equal to the distance from an erosional site (eroding bank) to the next depositional site (point bar) downstream. Many others have observed similar relationships based on the spacing of erosional and depositional sites and channel morphology (Beechie, 2001; Pyrcz and Ashmore, 2003a, b; Hundey and Ashmore, 2009; Kasprak et al., 2015; Vázquez-Tarrío et al., 2019). Further, depositional areas (typically bars), have demonstrated a higher probability of 'trapping' particles than erosional morphological units (McDowell and Hassan, 2020; McDowell et al., 2021). Finally, experimental research has confirmed the preferential deposition of particles specifically at bar heads and margins even in channels with more complex morphology, for example, in braided rivers (Kasprak et al., 2015) but it is reasonable to assume that in multithreaded channels, multiple path lengths might exist at different flow stages in primary and secondary channels.

Where  $L$  is the distance the particles travel and  $T$  is the time over which the particles are traveling, Vericat et al. (2017) proposed an equation to use the path length with the volume of erosion derived directly from the DoD

$$Q_b = (v_b \cdot \sum V_e) \quad (1)$$

The path length used for the virtual velocity approach is generally taken as the mean travel distance (Wilcock, 1997; Vericat et al., 2017; Mao et al., 2017; Brenna et al., 2019). However, it is unclear if the mean path length as measured by tracers is the best representation of a 'characteristic' path length to estimate bedload transport. To obtain an estimate of reach scale sediment transport we consider the distance travelled by the bedload involved in building geomorphic units as representative a characteristic path length. This may not necessarily be the average, as evidenced by the wide variety of path length distributions it is often the case that many or even most (the mode) of path lengths are very short, thus skewing the average depending on the distribution. For example, Pyrcz and Ashmore published synthesis of tracer studies and demonstrated that at formative discharges, particle path length distributions often exhibit primary or secondary modes corresponding to the location of bars, where deposition occurs (Pyrcz and Ashmore, 2003a). Further, flume experiments showed that the majority of particles eroded from an upstream scour pool were deposited at the point bar apex and corresponded to peaks in bi or multimodal path length distributions (Pyrcz and Ashmore, 2005). Therefore, the characteristic path length, i.e., the most representative and sound value to be used in sediment transport estimations, might be better described by these primary or secondary modes in channels with bar morphology at channel forming flows.

If a characteristic path length can be inferred from changes in morphology as previously discussed, advances in topographic survey techniques to acquire detailed digital elevation models (DEMs) and facilitate change detection, provide an opportunity to streamline the estimation of sediment transport. The high-resolution topography (HRT) revolution (Vericat et al., 2017) has provided an abundance of high quality surveys and an increased frequency of change detection based on the differencing of DEMs to create digital elevation models of difference (DoDs) (Brasington et al., 2000; Lane et al., 2003). Vericat et al. (2017) proposed an equation to use the path length with the volume of erosion derived directly from the DoD

$$Q_b = (v_b \sum V_e (1 - p)\rho_s)/L_c \quad (3)$$

Where  $\sum V_e$  is the total volume of erosion from the DoD and  $L_c$  is the length of the analyzed DEM by which the volume of erosion is normalized (Vericat et al., 2017). To use this method,  $L_c$  must be long enough for average path lengths ( $L$ ) to occur and  $T$  must be short enough to prevent repeated erosion and deposition, known as compensation (Lindsay and Ashmore, 2002).

Redolfi (2014) attempted to estimate the path length parameter directly from the DoD using the length of individual erosional patches as a proxy for the length of the erosion-deposition sequence. This approach avoids the need to couple each erosional area to a downstream depositional area, which can be difficult to automate in multi-thread rivers. While this method scales well with flow metrics and provides reasonable estimates (Redolfi, 2014; Vericat et al., 2017), the hypothesis that the length of erosional areas is equivalent to the erosion-deposition distance has not been tested in different morphologies, and it is not clear how the survey resolution may affect the estimates by fragmenting the erosional areas into smaller parts. Recently, Calle et al. (2020) used a method of river segmentation to visualize the pattern of erosion and deposition and infer sediment connectivity as well as to estimate potential travel distances. They defined boundaries between river segments and classified them into types based on their net erosional or depositional characteristics. Focusing on the "type 1 depositional boundary" wherein the upstream section is erosional and the immediate downstream boundary is depositional and depending on the volumes of deposition and erosion in these segments they were able to estimate minimum or maximum transport distances (Calle et al., 2020). This approach provides greater insight into the spatial connectivity of the river corridor and is useful to understand reach scale processes. However, depending on the river, and the sections surveyed, the number of type 1 boundaries may limit the applicability of the method in defining a characteristic path length and crucial information may be missed where the pattern of erosion and deposition is not clear, or the periodicity spans multiple sections. For example, where there are back-to-back patches of erosion or deposition or the overall pattern is separated by small areas of mixed boundaries.

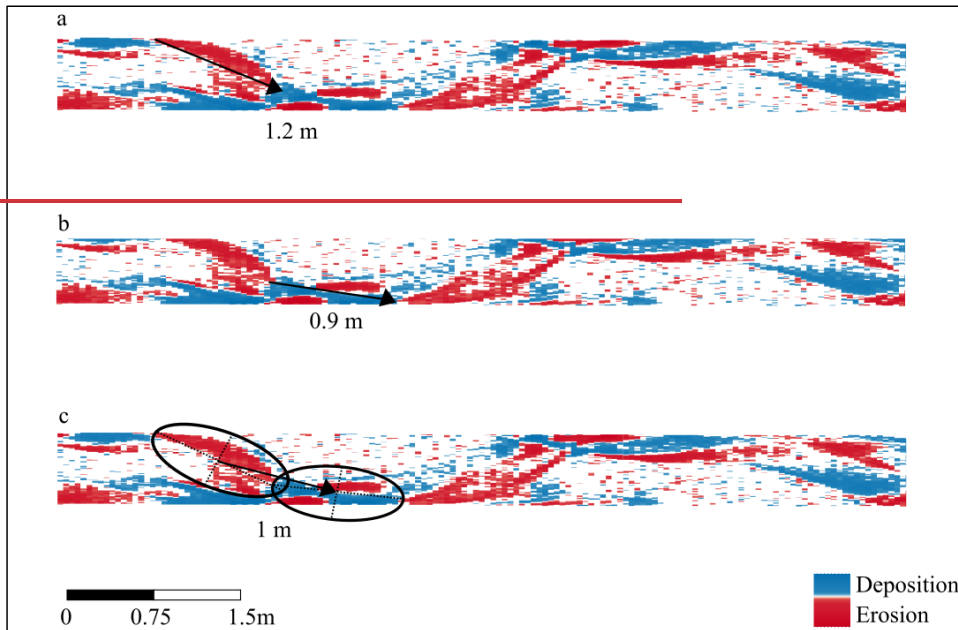
Given the observations linking path length to morphology and building on the aforementioned methods, we seek to expand on the idea that characteristic path length can be inferred from changes in morphology at near transport event scale comparisons. If during a flood, sediment is mobilized from an area of erosion to an area of deposition as represented on the DoD, the distance between the two should correspond to a characteristic path length. Following these assumptions this work has the following objectives: i) to propose an objective and semiautomatic method to quantify a characteristic path length as represented by the periodic nature of erosion and deposition from the DoD using flume data; ii) to compare these estimates of a characteristic path length to measured path length distributions obtained from tracer data in the field; iii) and finally to evaluate the conditions in which a characteristic path length is appropriate to estimate sediment transport.

## 185 2 Methods

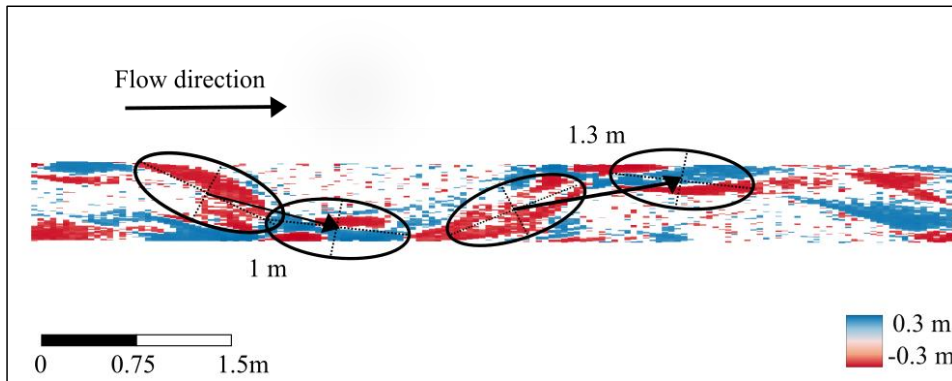
186 To meet our objectives, we use flume experiments at varying discharges with direct measurement of output sediment flux  
187 and sets of repeat DEMs from which DoDs are created and used to identify patterns of erosion and deposition. 2. We then  
188 develop a semiautomated method to extract these distances between erosion and deposition as a proxy for the  
189 characteristic path length and then compare our estimates of sediment flux calculated using the characteristic path length  
190 to measured sediment flux. Finally, we compare the characteristic path length estimates from a published case study to  
191 the physical path length distributions as measured by tracers in the field to see how the characteristic path length  
192 corresponds to path length distributions.

### 194 2.1 Path length

195  
196 The crux of our hypothesis is that sediment moves from an area of net erosion to an area of net deposition during the  
197 time period between DEM acquisitions and that this represents a characteristic path length. The most obvious method to  
198 quantify this distance between erosional and depositional sites on the DoD is to measure the spacing manually using a  
199 GIS program however, this requires many subjective evaluations. Firstly, we must decide where on the patches of  
200 erosion and deposition to begin and end the measurements. Because patches of erosion and deposition are not  
201 symmetrical or of equal size, the distance between the two depends on which area of the patch we choose to begin and  
202 end the measurements (Fig. 1). For consistency, we choose the center of the patch (Fig. 1c). Next, we must determine  
203 which patch of erosion matches with which patch of deposition which is not always obvious, especially when multiple  
204 channels are present, and again requires subjective evaluation. Here we used our knowledge of morphological processes  
205 to make a best estimate. For example, a patch of erosion on an outside bend likely corresponds to the deposition of the  
206 next point bar downstream. Although this method is capable of producing estimates of path length, to overcome the  
207 subjectivity and time required to manually measure the distances we developed a method to extract the spacing that is  
208 objective and semiautomated.



209  
 210 A key assumption inherent in our objectives is that sediment moves from an area of net erosion to an area of net  
 211 deposition during the time period between DEM acquisitions and that this represents a characteristic path length.  
 212 Ferguson and Ashworth (1992) proposed a similar method of matching specific erosional and depositional patches  
 213 albeit without the assistance of a DoD. This method was then implemented in the Sunwapta River, Canada (Goff and  
 214 Ashmore, 1994) although the authors note the difficulty in finding perfectly matching patches and conclude that  
 215 erosional and depositional processes are likely more dispersed. Here we will implement this “manual method” as a  
 216 means of comparison for the automated method presented later. The most obvious method to quantify this distance  
 217 between erosional and depositional sites on the DoD is to measure the spacing manually using a GIS program however,  
 218 this requires many subjective evaluations. Firstly, we must decide where on the patches of erosion and deposition to  
 219 begin and end the measurements. Because patches of erosion and deposition are not symmetrical or of equal size, the  
 220 distance between the two depends on which area of the patch we choose to begin and end the measurements. For  
 221 consistency, we choose the center of the patch (Fig. 1) after Ashmore and Church (1998). Next, we must determine  
 222 which patch of erosion matches with which patch of deposition which is not always obvious, and as noted previously,  
 223 likely does not accurately represent the nature of bedload transport (Goff and Ashmore, 1994). Here we perform this  
 224 method solely for comparative purposes and therefore used our knowledge of morphological processes to make a best  
 225 estimate. For example, a patch of erosion on an outside bend likely corresponds to the deposition of the next point bar  
 226 downstream (Fig. 1). Although this method is capable of producing crude estimates of path length to overcome the  
 227 aforementioned biases (Ferguson and Ashworth, 1992; Goff and Ashmore, 1994; Ashmore and Church, 1998) we  
 228 propose a method to estimate a characteristic path length without relying on the matching of erosion and deposition but  
 229 rather to use the periodic nature of these processes. Additionally, we seek to create a method that is both objective and  
 230 semiautomated.

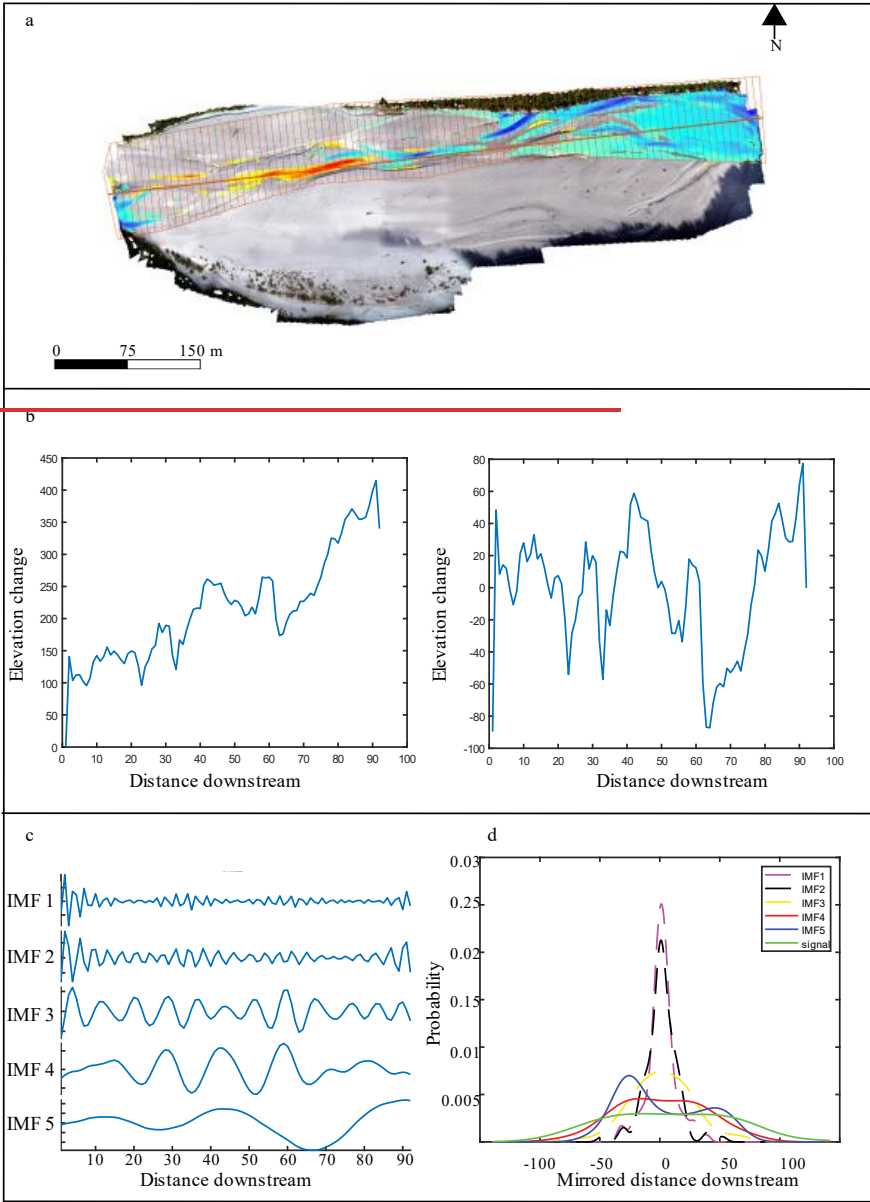


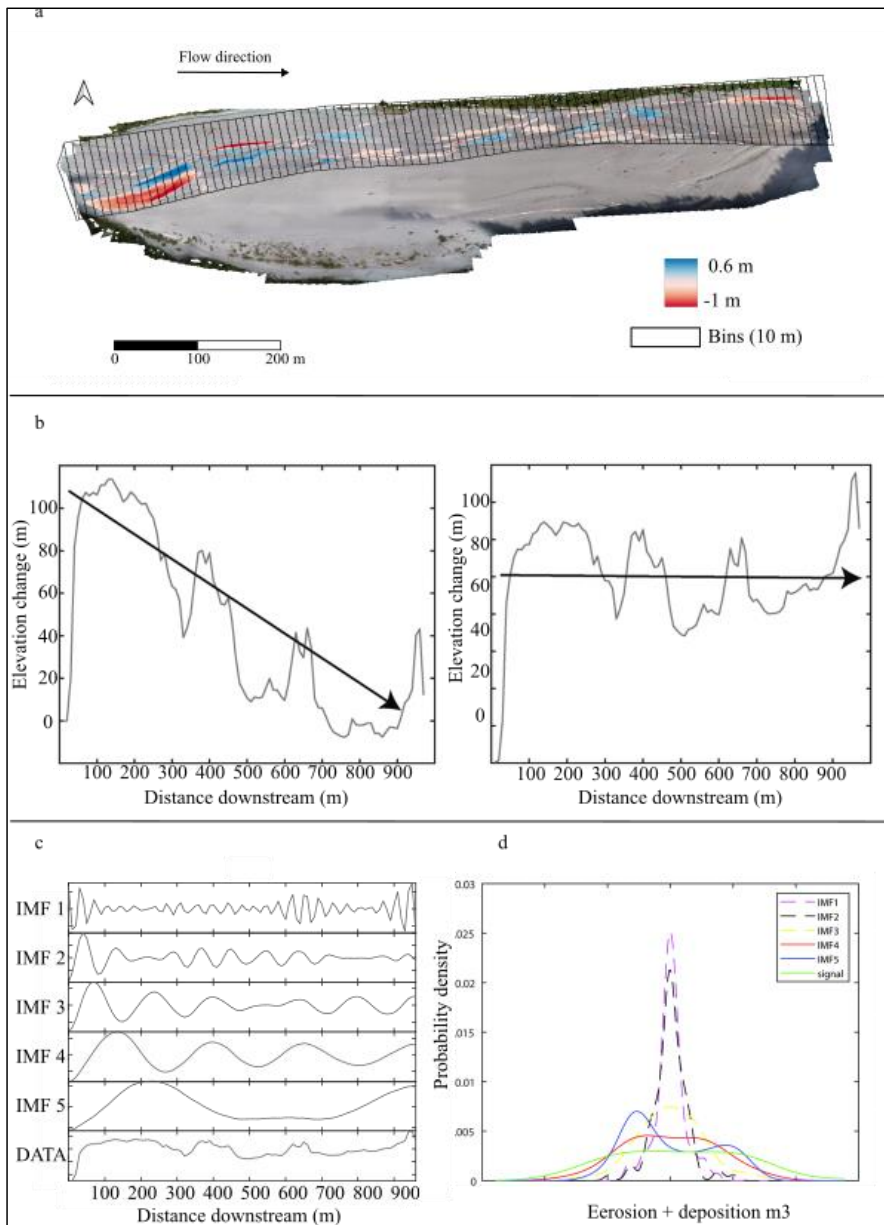
231  
232 **Figure 1: Manual method to measure spacing of erosional patches (red) and depositional patches (blue) on a**  
233 **DoD. (a) Beginning-of-patch-to-beginning-of-next-patch (b) end-to-end (c) center-to-center.**  
234

### 235 2.3.2 Semiautomated extraction of path length

236  
237 To visualize and then quantify the spacing/periodic nature of erosional/erosion and depositional sites on deposition from  
238 the DoD we simplify the spatial heterogeneity of the DoD into a vector of the net change in elevation in a streamwise  
239 direction (Fig. 2a). Because natural rivers are rarely straight, for field case studies, we must enforce a linear downstream  
240 directionality essentially straightening the bends in the river. This is achieved by segmenting the DoD into a series of  
241 equally sized “bins” using the segmentation tool of the Fluvial Corridor Toolbox (Roux et al., 2015) (Fig. 2a). We then  
242 sum the values in each bin to obtain a vector of the net change in elevation in a streamwise direction (Fig. 2b). In the  
243 flume studies, where there is no sinuosity, we simply sum each column of the DoD matrix. The bin size can affect the  
244 pattern of erosion and deposition in that by selecting too large of bins we may miss important erosional or depositional  
245 areas when they are summed in the same bin. Similar methods that require river segmentation have proposed using the  
246 reach averaged width for the length of the bins (McDowell et al., 2021) or half of the width of the reach (McDowell and  
247 Hassan, 2020) although these studies had different objectives. Calle et al. (2020) applied a segmentation method with a  
248 similar goal of identifying corresponding zones of erosion and deposition and set the bin sized based an assessment of  
249 the river dimensions as well as the minimum transfer distance of interest. Therefore, depending on the river, the user  
250 may select differently sized bins. Once the river is segmented, we then sum the values in each bin to obtain a vector of  
251 the net change in elevation in a downstream direction (Fig. 2b). In the flume studies, where there is no sinuosity, we  
252 simply sum each cross section of the DoD matrix. Oftentimes a reach is aggrading or incising and therefore the net  
253 vector will have an increasing or decreasing trend (Fig. 2b). Because we are interested in the spacing between areas of  
254 erosion and deposition rather than the overall trend, we remove it by subtracting a best-fit linear trend from the net  
255 vector (Fig. 2b). Because we simplify the heterogeneity of erosion and deposition into a net vector of elevation change,  
256 we risk compensating erosion and deposition within the same cross section, therefore we also create a vector of just  
257 erosion and one of just deposition as well as the net allowing for a visual comparison of the relative contribution of  
258 erosion and deposition to the net as well as the periodicity of the individual processes (Fig. A1). We can see that there  
259 appears to be a periodicity as the net vector oscillates forming peaks and troughs and although this periodicity seems  
260 apparent, quantifying the distance is not straightforward.







262

263

264

265

Figure 2: VMD- HD method (a) Segmentation of the DoD. (example orthophoto and DoD from the Tagliamento River, Italy), (b) Plot of the net original and detrended vector. (c) Variational mode decomposition (VMD) with 5 intrinsic mode functions (IMFs). (d) Probability density function (PDF) of each IMF and the original net vector.

266

267

From Fig. 2b, it is clear that One approach could be to count the pattern of erosion zero crossings and deposition exhibits then use that distance as the proxy for path length. However, we risk measuring low magnitude spikes that cross

268 zero that may not necessarily represent the overall periodicity or large oscillations that don't cross the zero line. A  
 269 smoothing filter may be used to remove these low magnitude oscillations but there is also variation and "noise".we risk  
 270 losing potentially relevant information. To see the pattern more clearly and quantify the periodicity solve this problem,  
 271 we turn to the field realm of signal processing where the problem of de-noising practice of "denoising" and extracting  
 272 information from oscillations is ubiquitous.

273 Signal processing is a field that deals regularly with extracting information and patterns that are not visually apparent  
 274 and its applications have been used in a wide variety of settings including voice recognition (Sigmund, 2003; Upadhyay  
 275 and Pachori, 2015), medical applications (Boudraa et al., 2005; Liu et al., 2008), and even time series analysis of  
 276 climate data (Barnhart and Eichinger, 2011). There are many approaches to de-noising including Fast Fourier transform,  
 277 empirical mode decomposition (EMD), and wavelet analysis. Each of these methods come with inherent strengths and  
 278 weaknesses, for example wavelet analysis requires that a mother wavelet be selected a priori and may influence the  
 279 results (Boudraa et al., 2005). We chose to use variational mode decomposition (VMD) due to its robustness with  
 280 respect to sampling and noise and the ability to handle signals that exhibit non-linearity and non-stationarity  
 281 (Dragomiretskiy and Zosso, 2014; Huang et al., 2016; Ma et al., 2017). VMD decomposes the signal into a set of  
 282 intrinsic mode functions (IMFs) each with a different central frequency (Dragomiretskiy and Zosso, 2014; Ma et al.,  
 283 2017) (Fig. 2c). In this case of our static 'signal' the frequency is more accurately described as the wavelength. It is  
 284 beyond the scope of this paper to describe the mathematics of VMD in detail, therefore, for a complete explanation see  
 285 (Dragomiretskiy and Zosso, 2014; Huang et al., 2016; Ma et al., 2017; Upadhyay and Pachori, 2015).

286 Once the original net vector of erosion and deposition is decomposed into the various IMFs, we need to select the IMF  
 287 or IMFs that most accurately represent the periodicity of the original data and therefore our characteristic path length.  
 288 Ma et al. (2017) proposed a method to select the most relevant IMF, and therefore periodicity of the signal, by  
 289 computing the probability density function (PDF) using kernel density smoothing for each of the five IMFs and of the  
 290 original data vector (Fig. 2d), then to calculate the Hausdorff distance (HD), a metric of geometric similarity, between  
 291 each IMF's PDF and the PDF of the original data and select the IMF most geometrically similar to the original data (Ma  
 292 et al., 2017) (hereafter VMD-HD method). In most cases, the longer wavelength IMFs most closely resemble the  
 293 original signal whereas the IMFs with shorter wavelengths are more likely associated with noise (Boudraa et al., 2005).  
 294 The computed wavelength is converted to a meaningful physical quantity by multiplying by the bin spacing in meters.  
 295 Because we are interested in the distance from peak to trough, we divide the period by two to obtain the path length  
 296 proxy (Neill, 1971; Ashmore and Church, 1998). Although this method allows for the selection of one IMF to  
 297 presumably represent the periodicity of the data, we record path lengths calculated from the other IMFs to evaluate the  
 298 range of estimates generated by the decomposition and determine if the VMD-HD method is appropriate for  
 299 determining a characteristic path length and the relative importance of other IMFs. All calculations were performed in  
 300 MatLabR2020b- using the built in VMD function and the Hausdorff distance function (Danziger, 2023).

301 One important consideration when using VMD to decompose a signal is that is the user must define the number of IMFs  
 302 beforehand. The number of IMFs is important as under binning, choosing too few IMFs, may mean that critical IMFs  
 303 are missed, whereas over binning, can cause duplication of components (Wu et al., 2020). In signal processing, there are  
 304 sophisticated methods for determining the number of IMFs, for a summary see (Wu et al., 2020). However, for our  
 305 purposes and simplicity's sake, we performed a brief sensitivity analysis based on the property of convergence often  
 306 used in the signal processing methods (Wu et al., 2020; Huang et al., 2016; Ma et al., 2017). The default setting in the  
 307 MatLab function is 5 IMFs, we used 3, 5, 8, 15, and 25 IMFs to calculate path length and assessed how it changed for

the maximum IMF (Fig. A2). We found that using more IMFs generally increased the number of high frequency components rather than the lower frequency IMFs (Fig. A3). Because these higher frequencies are generally associated with noise and in our case are physically too small to likely represent meaningful path lengths (on the order of millimeters) we decided more than 5 IMFs did not contribute physically meaningful information in that the IMFs with longer wavelengths did not change drastically. We also determined that 3 IMFs were too few as it was clear that the longer wavelengths were missing (Fig. A3). Therefore, we chose to use the default 5 IMFs as this provided a manageable number of components while effectively separating the lower frequencies. This is a convenient starting point for assessing the VMD method as a tool to extract the periodicity as a proxy for characteristic path length but is by no means the only option. We encourage further exploration of the IMF parameter in future applications and as the method is refined.

### 3 Flume and field data

The method was tested using data from a set of flume runs performed in the Hydraulic Laboratory of the University of Trento, where DEMs were generated for fixed time intervals and varying discharges, and direct measurements of the bedload flux were also collected. To test the efficacy of the method in the field, we selected a published dataset of measured path lengths with corresponding DoDs for the San Juan River in British Columbia Canada (McQueen et al., 2021). In this case, DoDs and corresponding tracer data were available for three separate bars (bar 6, bar 7, and bar 15) for the 2018-2019 period. Although McQueen et al. deployed tracers in four separate periods, there was only one deployment (2018-2019) with corresponding DEMs (McQueen et al., 2021). DoDs and corresponding tracer data were available for three separate sites (bar 6, bar 7, and bar 15) for the 2018-2019 period. Detailed information on their collection and processing can be found in McQueen et al., 2021.

#### 3.1 Flume experiments

The Trento laboratory experiments were carried out in a 0.6 m wide and 24 m long flume, filled with sand characterized by a median nearly uniform 1 mm diameter ( $D_{50}$ ) of 1 mm sand. The flume slope was set to 0.01 m/m. Topographic surveys were performed over the final 14 m of the flume, to limit the upstream inflow effects, using a laser gauge, mounted on a movable deck. The longitudinal and crosswise spacings were 0.05 m and 0.005 m, respectively. Four sets of nine runs were performed, with the flow discharge set to 0.7, 1, 1.5, and 2 l/s, which correspond to a range of different planform morphologies (see Fig. 3-Table 1). Sediment input at the upstream end of the flume was constant in each run, with a flux equal to the average measured at the downstream end, as computed in a preliminary set of experiments. Therefore, the overall average bed elevation of the runs was in equilibrium, with no net erosion or deposition. The runs were performed following the same procedure, involving three phases of different lengths, based on the transport condition of each discharge. These durations were estimated referring to the time scale for morphological evolution computed from the sediment balance mass equation (Garcia Lugo et al., 2015), which can be expressed as:

$$T_{ex} = \frac{DW^2}{Q_b}, \quad (4)$$

where D is the average flow depth and W is the flow width. Table 1 provides the values of  $T_{ex}$  for each flume experiment.

**Table 1: Initial conditions for each dataset including the type of validation data.**

	Flume 1	Flume 2	Flume 3	Flume 4	San Juan Bar 6	San Juan Bar 7	San Juan Bar 15
Peak discharge (m <sup>3</sup> /s)	0.0007	0.001	0.0015	0.002	942	942	942
Slope (m/m)	0.01	0.01	0.01	0.01	0.0038	0.0031	0.0009
Width (m)	0.6	0.6	0.6	0.6	150	150	130
D <sub>50</sub> (m)	0.001	0.001	0.001	0.001	0.05	0.056	0.042
Time scale T <sub>ex</sub> (min) (eq.4)	94	50	38	30	-	-	-
Time between surveys (0.5 T <sub>exmin</sub> )	47	25	19	15	~1 year	~1 year	~1 year
ω* Dimensionless stream power	0.15	0.22	0.33	0.43	0.76	0.61	0.31
Validation Data	Sediment Flux	Sediment Flux	Sediment Flux	Sediment Flux	RFID tracers	RFID tracers	RFID tracers
Planform	Wandering	Wandering	Wandering transitional	Alternate bar	Wandering	Wandering	Wandering

Formatted Table

345

346 First, an initial phase of about 12 times this time scale  $T_{ex}$  with constant flow was run, to ensure the formation of a  
 347 near-equilibrium morphological condition, starting from a flat sand bed scraped to the prescribed slope. This was  
 348 followed by a long run, at constant discharge, lasting 19 times the time scale  $T_{ex}$ , aimed at measuring the output  
 349 sediment flux. This was continuously monitored at the channel outlet, through a permeable basket placed on four load  
 350 cells. Sediment flux was measured every minute. After a bed topography survey, the third phase was a sequence of nine  
 351 shorter runs, lasting 0.5 times the time scale  $T_{ex}$ , each followed by a bed topography survey, which produced nine  
 352 corresponding DoDs. The duration of these nine runs (and therefore the time interval between surveys) was decided to  
 353 have easily measurable changes of the bed morphology, without having significant compensation processes. ~~The use of~~  
 354 ~~the time scale  $T_{ex}$  (and therefore a different absolute time interval between surveys for the four discharges) ensured to~~  
 355 ~~have similar volumes of erosion and deposition in each run.~~

356 The DoDs were created by subtracting two consecutive DEMs, then underwent a three-step filtering process to highlight  
 357 the relevant erosion and deposition patterns, removing most of the noise associated with the surface roughness and  
 358 measurement accuracy. First, the DoDs were filtered considering a uniform detection threshold equal to 2 mm (2 times  
 359 the  $D_{50}$ ), meaning that erosion or deposition values lower than this threshold are set to zero. Thereafter, a spatial average  
 360 was performed as a moving average on three values along the transversal direction where the DoD discretization is the  
 361 finest. Lastly, a despeckling algorithm removed all isolated cells, both considering single cells that show erosion or  
 362 deposition, as well as single cells that show no change. This last step was implemented to keep the detection threshold  
 363 as low as possible while removing unphysically small areas. Additionally, we calculated the morphological active  
 364 width by determining the percentage of the DoD that showed morphological activity (i.e., was not zero after filtering).

### 365 3.2 San Juan River data

366 ~~To compare the characteristic path length to measured path length distributions in the field, we used data from the San~~  
 367 ~~Juan River, located on Vancouver Island, British Columbia with a drainage area of approximately 730 km<sup>2</sup> and a mainly~~  
 368 ~~rainfall driven hydrology (McQueen et al., 2021). The reach of interest in this study was alluvial in nature with a~~  
 369 ~~wandering morphology and a substrate composed of gravel, cobble, and sand (McQueen et al., 2021). The San Juan~~  
 370 ~~River DoDs were downloaded directly from the Scholars Portal Dataverse (<https://doi.org/10.5683/SP2/UQGZCG>). The~~  
 371 time in between acquisitions is one year, in which it is estimated there were five flood events able to generate sediment

transport using a threshold of 500 m<sup>3</sup> s<sup>-1</sup>, which was visually estimated by the authors to be equivalent to the bankfull discharge (McQueen et al., 2021). DEMs were generated by LIDAR acquisitions and have a spatial resolution of 10 cm and a vertical root mean square error lower than 10 cm. Topographic changes between survey dates were then calculated by processing the LiDAR DEMs using the Geomorphic Change Detection (GCD) software (Wheaton et al., 2010). More information on how they were obtained and processed including the spatially variable thresholding techniques can be found in McQueen et al. (2021). The LiDAR-derived DoDs were used to interpret patterns of tracer displacement and burial depths and to provide information on the morphological development of the bars during the study period. However, they do not provide complete reach-scale sediment budgets due to the lack of in-channel topographic data and stage differences during each LiDAR survey affecting the relative portion of the river bed that was exposed. Nevertheless, we believe the exposed part of the channel, the bars, and associated patches of erosion and deposition (see Fig. 9b) are sufficient to be used with our proposed method to estimate path lengths and be compared with field measured path lengths from the tracer data. This is because we are not calculating sediment flux for the San Juan River and are only interested in comparing our estimates of the characteristic path length to the measured tracer distributions. As far as the pattern of erosion and deposition and how that may be disrupted, we believe that because the submerged area is small relative to the DoD the pattern should not change drastically. Further, by looking at figures 15 and 16 from McQueen et al. (2021) we can see that the tracers were largely recovered from the exposed bar surfaces in the 2018-2019 deployment. This gives us confidence that the deposition we are measuring corresponds largely to the deposition associated with the tracers. Although this is not an ideal situation, we believe the benefits outweigh the limitations considering the difficulty of finding high quality RFID tracer data and corresponding DoDs. The San Juan River DoDs were downloaded directly from the Scholars Portal Dataverse (<https://doi.org/10.5683/SP2/UQGZCG>), are sufficient to be used with our proposed method to estimate path lengths and be compared with field measured path lengths from the tracer data. The DoDs were segmented using similar principles to Calle et al. (2020) in a similarly sized river, therefore the bin size was conservatively set at 10 m.

### 3.3 Validation data and error estimation

Each study had unique initial conditions including slope, discharge, grain size, channel configurations, and time/flood events between surveys (Table 1). Because the studies vary with respect to these initial conditions, we calculated the dimensionless stream power ( $\omega^*$ ) after Bertoldi et al. (2009) to compare them as:

$$\omega^* = \frac{Q \cdot S}{W \sqrt{g \Delta D_{50}^3}} \quad (5)$$

where  $Q$  is the peak discharge,  $S$  is slope,  $W$  is the average wetted width,  $\Delta$  is the relative submerged density,  $D_{50}$  is the median grain size, and  $g$  is the acceleration due to gravity.

For the flumes, we used estimates of path length generated by the VMD-HD method and those associated with the two longest wavelengths, IMF 4 and IMF 5 separately to calculate the virtual velocity Eq. (2) and sediment flux Eq. (3) which we then compared to measured flux data. The measured sediment flux during the initial long run showed high variability, with phases of high and low sediment flux lasting several tens of minutes. For this reason, we prefer to use the data from the long runs, from which we estimated an average sediment flux of 0.33 g/s (SD=0.17) for the 0.7 l/s discharge, 0.78 g/s (SD=0.31) for the 1 l/s discharge, 1.98 g/s (SD=0.65) for the 1.5 l/s discharge, and 3.22 g/s

(SD=0.79) for the 2 l/s discharge (Fig. 3). We subdivided the second phase into 38 intervals of 0.5  $T_{ex}$  duration, equal to the duration as the short runs in phase 3, and computed the variability of the flux over this range.

We used ANOVA to compare path length, virtual velocity, and erosion across the four discharges ( $\alpha=0.05$ ) and a Post-hoc Tukey test to explore significant differences between discharges. To compare the measured sediment flux to the estimates from the VMD-HD method and the IMF 4 and IMF 5 estimates we used a student's t-test ( $\alpha=0.05$ ). And finally, to compare the error of our path length and sediment transport estimates we calculated the symmetrical mean absolute percent error (SMAPE)-relative percent error  $\delta$  in order to compare the sediment flux estimates to that of the long runs of average sediment flux as:

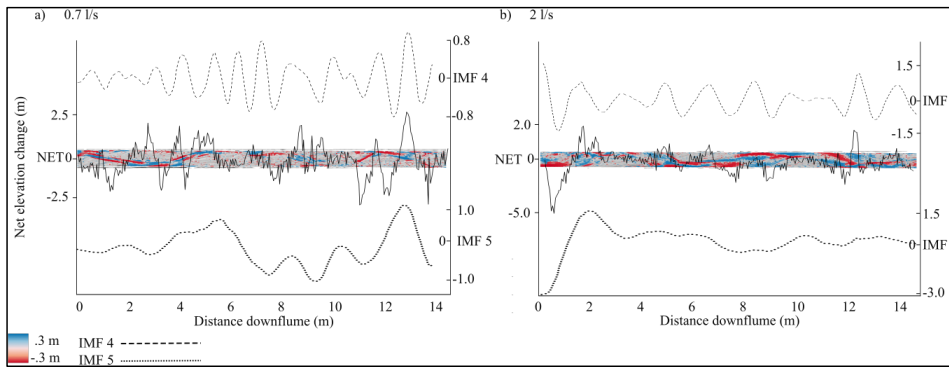
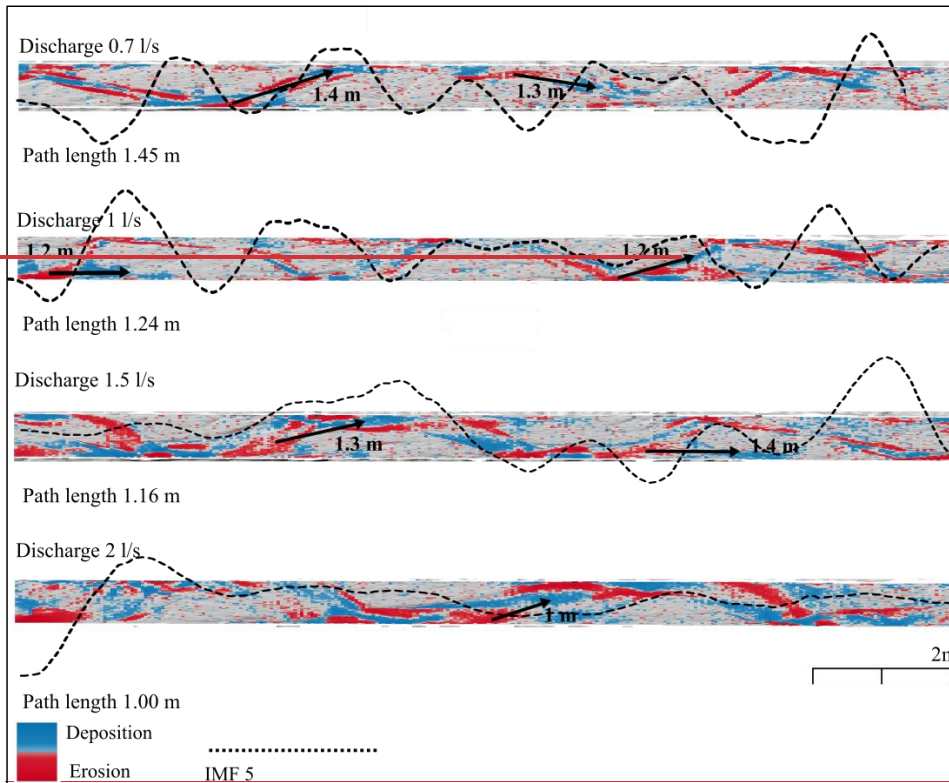
$$\delta = \frac{|E-M|}{M} \quad (6)$$

where  $E$  is the average of the estimated sediment flux for the 9 runs at a given discharge and  $M$  is the averaged measured sediment flux from the long run at the same given discharge. For the San Juan River we compared the VMD-HD estimates of path length and IMFs 4 and 5 qualitatively to the published path length distributions and the locations of mean, median, and modes. The tracer recovery locations were accessed in spreadsheet form and in keeping with the analysis of the authors we disregarded any tracers that moved less than 10 m before calculating the path length distributions.

## 4 Results

### 4.1 Flume experiment

To aid in the interpretation of the results, Fig. 3 shows a DoD from each of the discharges lowest discharge, 0.7 l/s (a) and the highest discharge, 2 l/s (b) with the IMF 5 net vector laid over the top (continuous line), IMF 4 (dashed line), and IMF 5 (dotted line) as obtained from the VMD method. Oftentimes the areas of deposition and erosion from the DoD correspond clearly to the IMF 4 and 5 vectors as with the 0.7 l/s discharge where areas of deposition are concave and areas of net erosion correspond to convex areas of the vector (Fig. 3a). At the higher discharges (1.5 l/s and 2 l/s) the total area of morphological activity increases and patches of erosion and deposition begin to overlap, creating a more chaotic and difficult to discern pattern (Fig. 3b, A1). We also observed a similar periodicity in the erosional and depositional vectors and at the 2 l/s discharge the depositional vector appears to show this most clearly (Fig. A1).

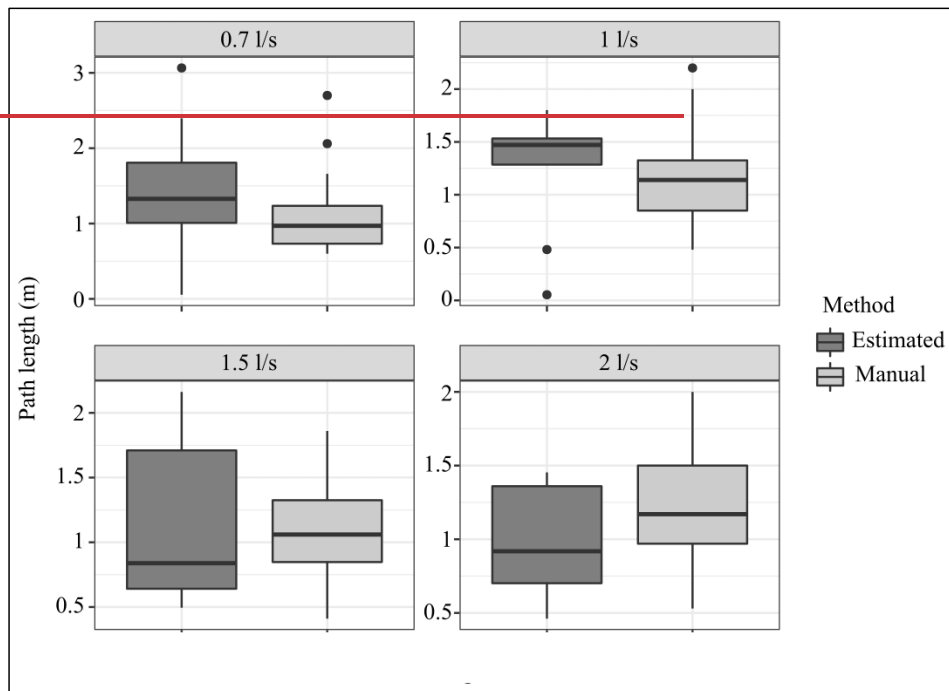


437 **Figure 3: All four discharges DoDs from the flume experiment DoDs 0.7 l/s discharge (a) and 2 l/s discharge (b)**  
 438 **with arrows showing manually derived distances from erosion to deposition, path-length estimates using the net**  
 439 **vector of elevation change laid over the VMD-HD method, and the top IMF 4 vector (above, dashed line) and**  
 440 **IMF 5 vector, (below, dotted line)**

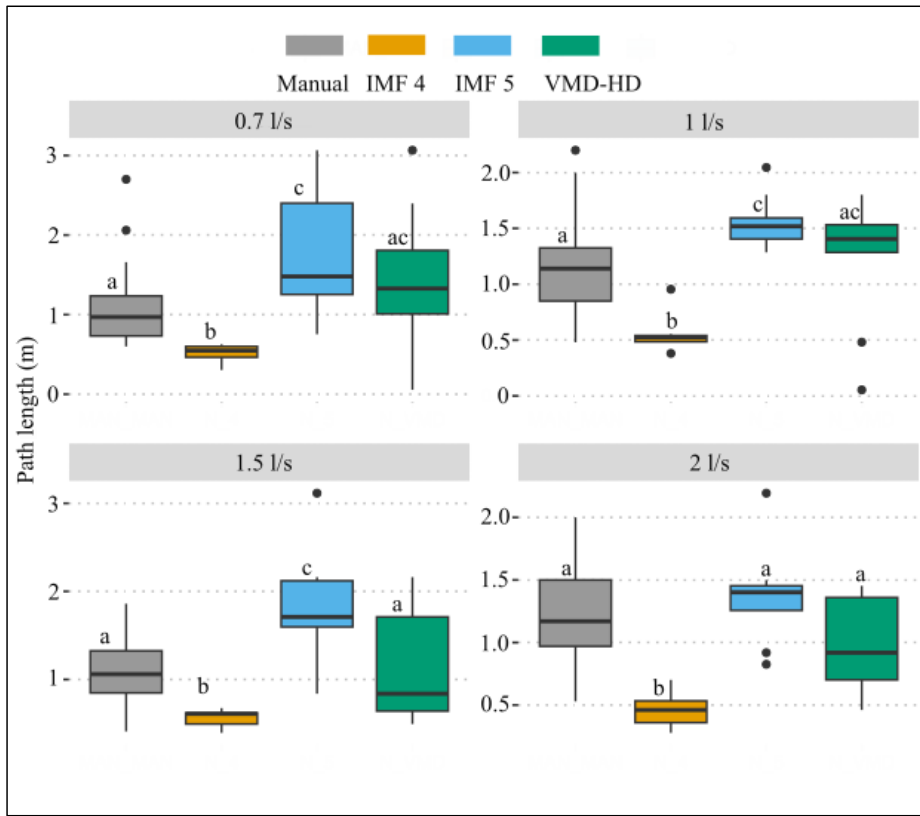
441 In the flume experiment, the VMD-HD method of choosing the most relevant IMF selected the longest wavelength IMF  
 442 5 7471% of the time and IMF 4 3423% of the time. IMFs 2 and 3 were never selected and IMF 1 was selected only  
 443 once-twice. However, at the higher discharges (1.5 l/s and 2 l/s) IMF 4 was selected more frequently, thereby reducing



444 the average path length when compared to the lower discharges (Fig. A4). Using the selected IMFs, the VMD-HD  
 445 method estimated a similar average path length for all of the discharges (Fig. 4 & 5). The averages were, 1.45 m  
 446 (standard deviation (SD) = 0.93) for the 0.7 l/s discharge runs, 1.24 m (SD=0.58) for the 1 l/s runs, 1.21 m (SD = 0.58)  
 447 for the 1.5 l/s runs, and 1 m (SD = 0.37) for the 2 l/s runs (Fig. 3). The path length estimates derived from the  
 448 path length estimates derived from IMF 4 were similar for all discharges, 0.51 m (SD=0.12) for the 0.7 l/s discharge,  
 449 0.55 m (SD=0.16) for the 1 l/s discharge, 0.56 m (SD=0.91) at the 1.5 l/s discharge, and 0.46 m (SD=0.15) at 2 l/s  
 450 (Fig.4) with no significant differences between the discharges ( $p > 0.05$ ). The path lengths derived from IMF 5 were  
 451 also similar between the discharges with no significant differences ( $p > 0.05$ ) and were, 1.75 m (SD=0.79) for the 0.7 l/s  
 452 discharge, 1.55 m (SD=0.24) for the 1 l/s discharge, 1.79 m (SD=0.67) for the 1.5 l/s discharge, and 1.37 m (SD=0.39)  
 453 for the 2 l/s discharge (Fig. 4). The VMD-HD method matched closely with the manually measured distances and there  
 454 were no statistically significant differences for any of the discharges ( $p$ -value  $> 0.05$ ) (Fig. 4-4) while the IMF 4 and  
 455 IMF 5 derived path lengths bracket the manually measured distances and the VMD-HD selected path lengths (Fig. 4).



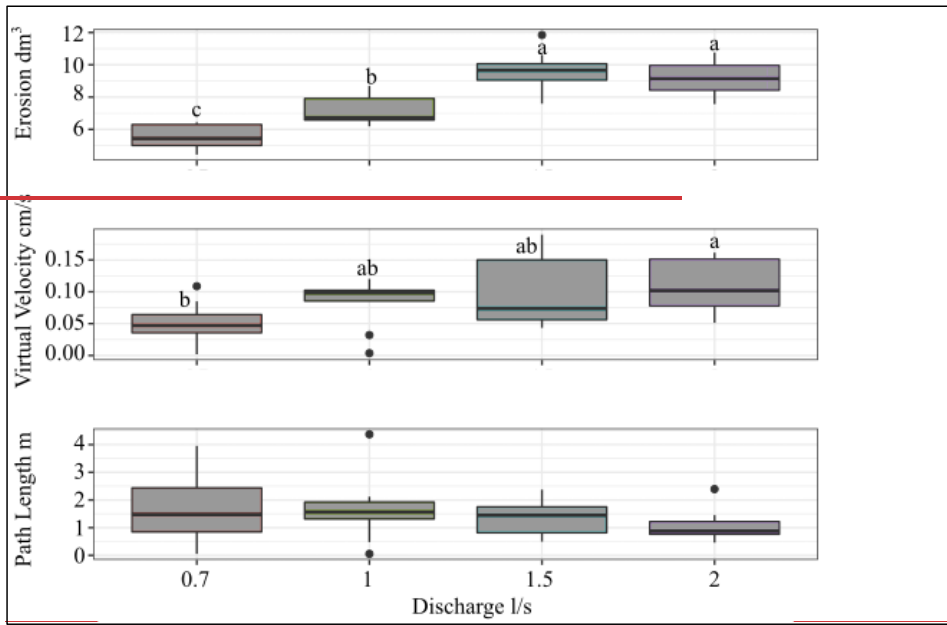
456

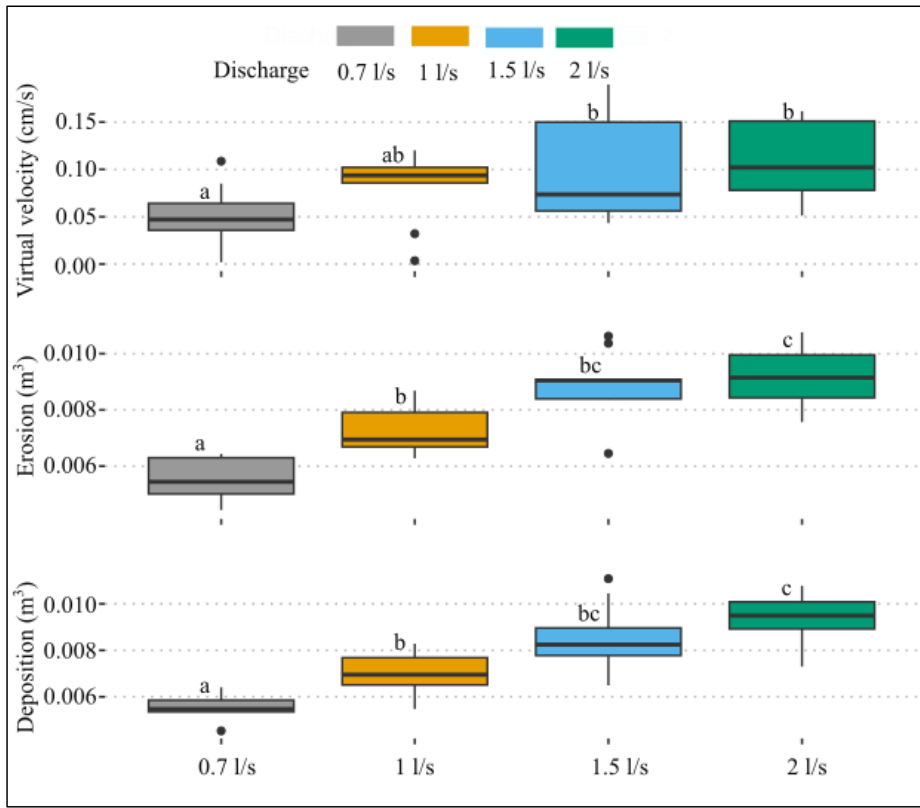


457

458 **Figure 4: Path length estimates from the manual method (gray), IMF 4 (orange), IMF 5 (blue), and the VMD-HD**  
 459 **method (dark gray) and the estimates derived green). Significant differences from the manual method (light**  
 460 **gray). The two groups were not statistically significant (p-value > 0.05); post-hoc Tukey test are denoted by letters**  
 461 **a-c.**

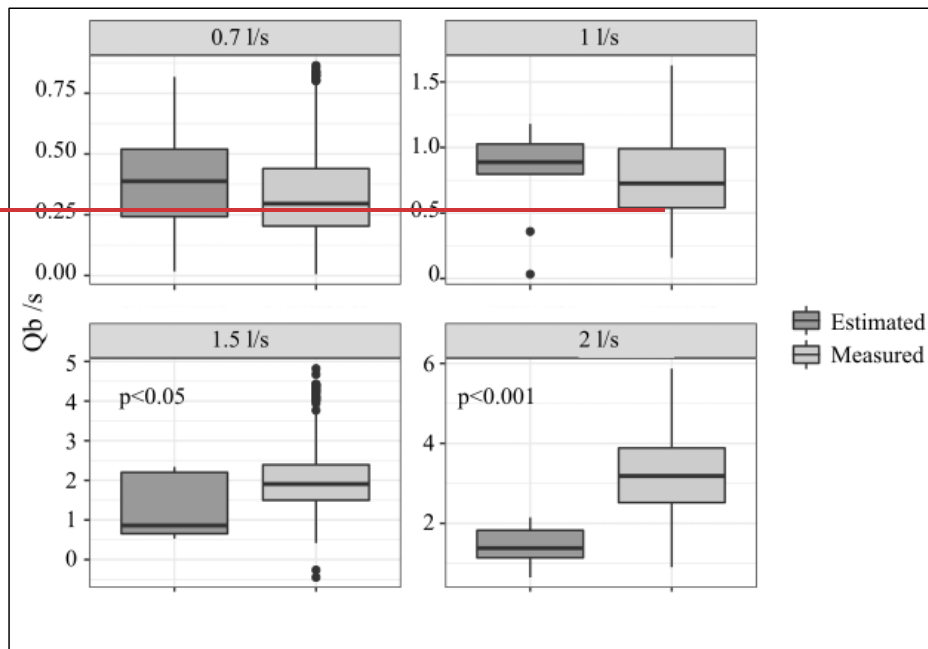
462 The estimated path lengths were not significantly different between the discharges (p-value > 0.05) (Fig. 5) and showed  
 463 no obvious trend of increasing or decreasing with discharge. However, when used to calculate the virtual velocity ( $v_b$ )  
 464 wherein the path length is divided by the time between surveys (Table 1), we see an increase in the virtual velocity with  
 465 discharge (p-value < 0.05) (Fig. 5). Likewise, the average ~~volume~~ volumes of erosion and deposition calculated from the  
 466 ~~filtered~~ DoDs increases significantly with discharge (p-value < 0.001) (Fig. 5).





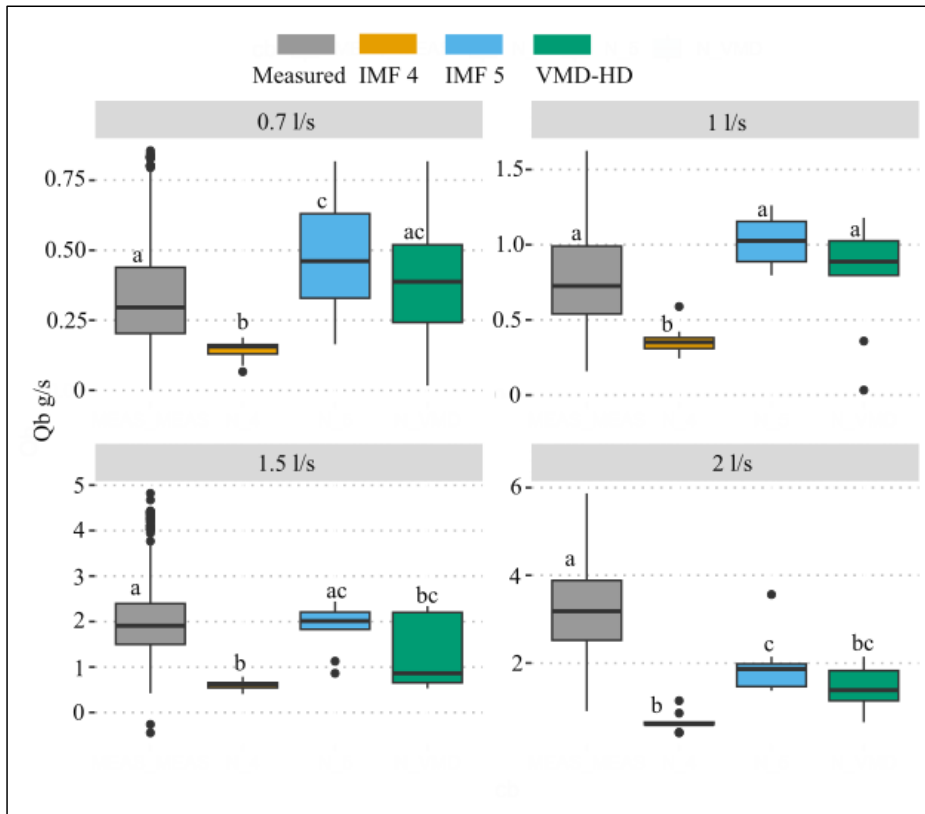
468  
469 **Figure 5: -Estimated path length using the VMD-HD method for all discharges in the flume experiment,**  
470 **calculated virtual velocity using these the VMD-HD path length estimates, and measured volumes of erosion and**  
471 **deposition for each discharge. Significant differences from the Post hoc Tukey test are denoted by letters a-c.**

472 When used to calculate sediment transport Eq. (3) the VMD-HD method corresponds well to the measured average for  
473 the lower discharges (0.7 l/s and 1 l/s) whereas at the higher discharges (1.5 l/s and 2 l/s) the method significantly  
474 underestimated the measured flux (Fig. 6). For the 0.7 l/s discharge, the VMD-HD method estimated a rate of 0.39 g/s  
475 (SD = 0.25) averaged over the nine runs, which was not significantly different than the measured average of 0.33 g/s  
476 (SD = 0.18) and the SMAPERelative percent error ( $\delta$ ) was 418%. For the 1 l/s discharge the method estimated 0.81 g/s  
477 (SD = 0.38) and was not significantly different than the measured average of 0.78 g/s (SD= 0.30) with a SMAPE of  
478 11%,  $\delta=4\%$ . At the higher discharge of 1.5 l/s the average estimated by the VMD-HD method was 1.2433 g/s (SD =  
479 0.4782) whereas the measured average was 1.98 g/s (SD = 0.70) (p-value < 0.05) with a SMAPE of 53%,  $\delta=32\%$ .  
480 Finally, for the 2 l/s runs the estimated average was 1.44g41g/s (SD = 0.4648) whereas the measured average was 3.22  
481 g/s (SD = 0.98) (p-value < 0.001),  $\delta=56\%$  (Fig. 6) with an SMAPE of 90%.



482  
483 **Figure 6: Estimated sediment flux (dark gray) compared to the measured average (light gray) for each of the 4**  
484 **discharges from the flume experiment. Significant p-values ( $\alpha < 0.05$ ) from a student's t-test are shown for the 1.5**  
485 **l/s and the 2 l/s discharges.**

486 If we use just the IMF with the longest wavelength (IMF 5) to estimate path length and calculate sediment transport, we  
487 slightly overestimate sediment transport at the 0.7 l/s discharge, 0.48 g/s although not significantly ( $p > 0.05$ ,  $\delta = 45\%$ )  
488 (Fig. 6). At the 1 l/s discharge IMF 5 significantly overestimates the average flux with an estimate of 1.03 g/s ( $p < 0.01$ ,  
489  $\delta = 32\%$ ). At the 1.5 l/s discharge the estimated flux of 1.88 g/s using the IMF 5 path lengths was not significantly  
490 different from the measured flux ( $p > 0.05$ ,  $\delta = 5\%$ ) (Fig. 6). However, using the IMF 5 path lengths still significantly  
491 underestimated sediment flux at the 2 l/s discharge, 1.95 g/s ( $p < 0.001$ ,  $\delta = 39\%$ ) (Fig. 6).

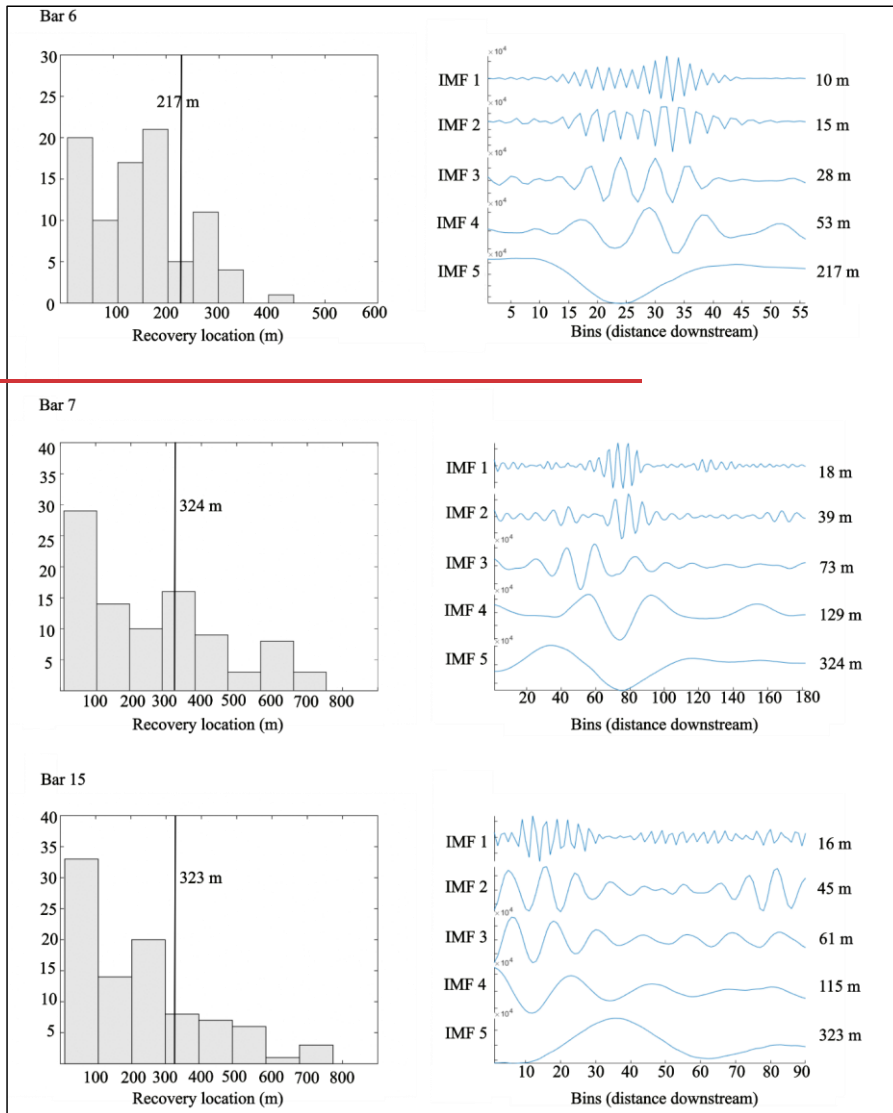


492 **Figure 6: Measured sediment flux (gray) compared to the estimates calculated using IMF 4 (orange), IMF 5**  
 493 **(blue), and the VMD-HD method (green). Significant differences from the post-hoc Tukey test are denoted by**  
 494 **letters a-c.**  
 495

496 Using the second longest wavelength, IMF 4, we underestimate at all of the discharges (Fig. 6). The estimated flux was  
 497 0.14 g/s at the 0.7 l/s discharge ( $\delta=58\%$ ), 0.36 g/s at the 1 l/s discharge ( $\delta=54\%$ ), 0.61 g/s at the 1.5 l/s discharge  
 498 ( $\delta=69\%$ ), and 0.65 g/s at the 2 l/s discharge ( $\delta=80\%$ ). (all p values  $<0.001$ ) (Fig. 6).

#### 499 4.2 San Juan River

500 For the three bars in the San Juan River dataset, the path length calculated from the VMD-HD method for bar 6 was  
 501 approximately 217 m whereas the field-measured average from tracers was 153 m (SMAPE=35%), and the mode range  
 502 was 150–200 m. For bar 7 the method-calculated a path length of 324 m whereas the measured-average was 255 m  
 503 (SMAPE=24%), and the secondary mode range was 280–380 m. Finally, for bar 15 the method-calculated a path-length  
 504 of 323 m whereas the measured-average was 221 m (SMAPE=38%), and the secondary mode range was 200–300 (Fig.  
 505 7).



506

507

508

509

510

511

512

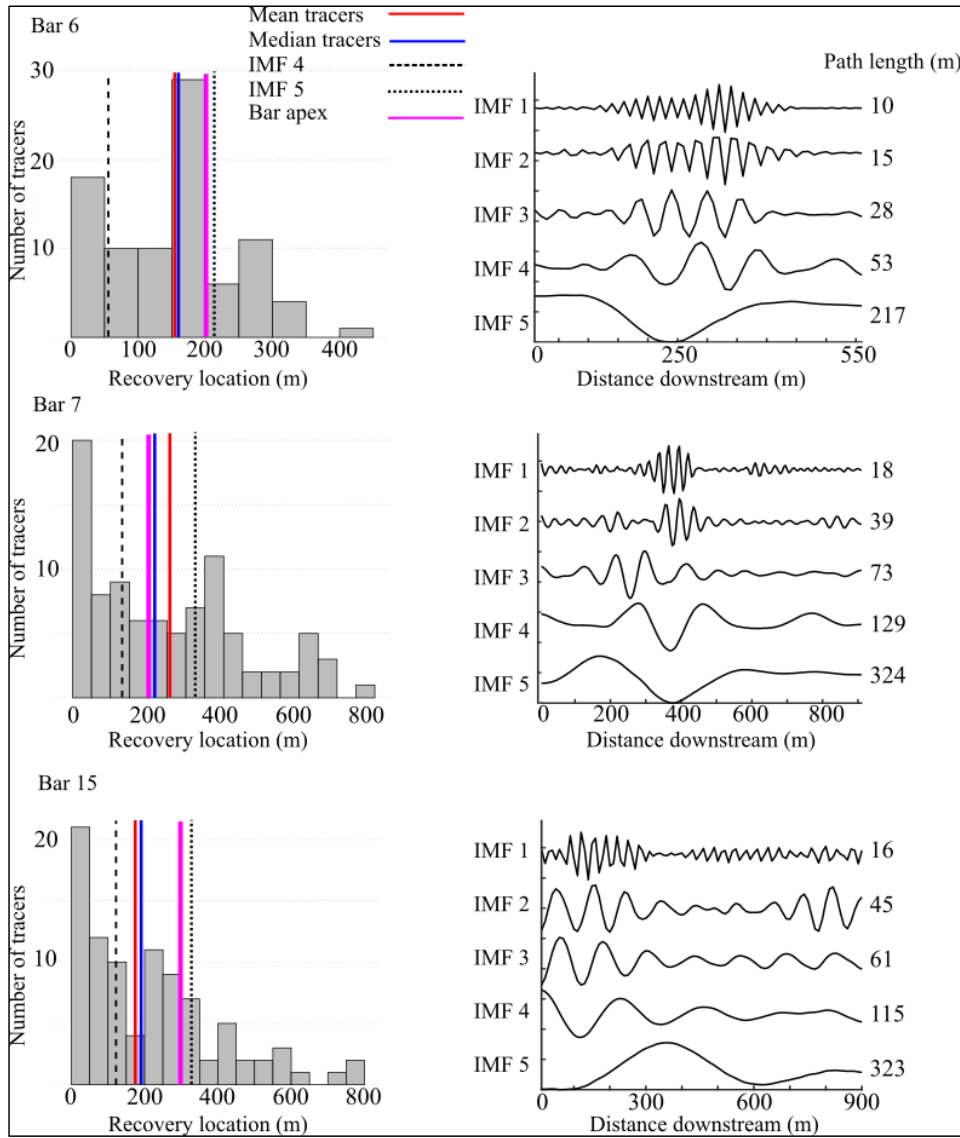
513

514

The 2018-2019 year for which we conducted our analyses, was moderate in terms of excess flow energy with 5 flood events exceeding a discharge of  $500 \text{ m}^3 \text{ s}^{-1}$  and a peak discharge of  $942 \text{ m}^3 \text{ s}^{-1}$ . The path length distributions of bar 7 and bar 15 are positively skewed although there is a secondary mode in the bar 7 distribution corresponding roughly to the bar tail (Fig. 7) whereas the distribution of bar 6 is bi-modal with the primary mode corresponding to the bar apex (Fig.7). This is potentially because bar 6 had the most pronounced curvature, perhaps contributing to the clustering of deposition just before the apex, where a migrating gravel sheet terminated (McQueen et al., 2021). This bar apex corresponds with the path length from IMF 5 of 217 m which was selected from the VMD-HD method (Fig. 7). IMF 5 was also selected by the VMD-HD method for bar 7 equaling 324 m, and here we see a correspondence to the small

515 secondary mode where the authors note there was a clustering of tracers (Fig. 7) (McQueen et al., 2021). Again, IMF 5  
516 with a path length of 323 m was also selected for bar 15 and corresponds closely to the bar apex, although there was not  
517 a clustering of tracer deposition in this deployment as observed in the year with higher discharge (Fig. 7). Additionally,  
518 bar 15 had the highest proportion of sand which is not represented by the tracers, potentially contributing to the  
519 discrepancy between our estimates and the tracers. IMF 4 was always well below the lengths associated with the bar  
520 apexes, and the median and mean tracer distances (Fig. 7). However, the bar apexes and the median and mean tracer  
521 distances were always between IMF 4 and IMF 5 (Fig. 7). The range between IMF 4 and IMF 5 accounted for 62% of  
522 the path length distribution for bar 6, 36% for bar 7, and 45% for bar 15.





523

524 **Figure 7: Tracers-based path length distributions (on the left) and VMD derived IMFs for bars 6,7, and 15 from**  
 525 **the San Juan River dataset. The VMD-HD method selected IMF 5 for all three bars and is reported on the**  
 526 **histograms on the left for visual comparison IMF 4 (dashed line), IMF 5 (dotted line), mean tracer distance (red),**  
 527 **median tracer distance (blue), and the bar apex (pink) are shown over the path length distributions.**

## 528 5 Discussion

529 We developed a method to estimate the characteristic path length during a given flood using information inherent to the  
 530 DoD by applying the principle that at channel-forming flows, the majority of particles move from an area of erosion to

the next area of deposition downstream (Pyrce and Ashmore, 2003a, b). By using the periodic nature of erosion and deposition we overcome the subjectivity and time involved in measuring these distances manually while aligning closely with these manually measured distances (Fig. 4). When evaluating the efficacy of our proposed method it is important to keep in mind the uncertainty of even direct measurement of sediment transport. The spatial and temporal frequency required to overcome the noise of measurement uncertainty (i.e., achieve an acceptable signal to noise ratio) in some cases can require sub-daily monitoring with precise equipment (Grams et al., 2019). The variability of sediment transport measurements in the flume study ranged from a standard deviation of approximately 30% to over 50% of the averaged flux (Fig. 6). Given this high variability, our reach scale averages were not significantly different from the measured averages for the 0.7 l/s and 1 l/s discharges (Fig. 6). We developed a method to estimate the representative path length during a given flood using information inherent to the DoD by applying the principle that at channel-forming flows, the majority of particles move from an area of erosion to the next area of deposition downstream (Pyrce and Ashmore, 2003b, a). Therefore, we hypothesized that the distance between net erosional and depositional sites should provide a reasonable estimate of the path length. Our method overcomes the subjectivity and time involved in measuring these distances manually while aligning closely with these manually measured distances (Fig. 4). Further, our estimates have an error lower than 30% when compared to the measured mode of tracer derived path length estimates in the field (Fig. 7). When used to calculate sediment flux our estimates are not significantly different than direct measurements of sediment flux for the lower discharge ranges in the lab (Fig. 6). Importantly, we observed that the method underestimates the sediment flux significantly for the two highest discharges in the lab where the bed shows a higher percentage of topographic change (Fig. 6). The method presented to estimate path length using only remotely sensed data shows promising results under certain conditions and provides insight into conditions where it is not applicable.

#### **5.1 Path length estimation by VMD-HD method: limitations and perspectives**

Importantly, we observed that the method underestimates the sediment flux significantly for the two highest discharges in the lab where the bed shows a higher percentage of the width experiencing topographic change (Fig. 6). The method presented to estimate a characteristic path length using only remotely sensed data shows promising results under certain conditions and provides insight into conditions where it is not applicable.

#### **5.1 Path length estimation by VMD-HD method: limitations and perspectives**

##### **5.1.1 Flow effects**

Previous studies have shown a relationship between path length and hydrologic variables such as discharge, stream power, and excess shear stress (Hassan et al., 1991; Pyrce and Ashmore, 2003b). A notable result of the flume experiment is that the estimated path length did not significantly differ between the four discharges (Fig. 4 & 5). We propose two possible explanations for this discrepancy with the literature. First, it is possible that the actual path length is increasing with discharge as has been observed in previous studies (Hassan et al., 1991; Pyrce and Ashmore, 2003b) but the method fails to capture it because the VMD-HD method is based on the spacing of erosion and deposition which does not change for the varying discharges under the flume conditions. It is possible that at higher discharges the characteristic path length, that we define as the distance from net erosional areas to net depositional areas, is not appropriate under the higher flow conditions because most particles are moving farther than the next depositional site downstream. This violates the assumption on which our method is based and is impossible to prove in our experiment without tracers. We can however look to literature to understand the conditions in which tracers tend to travel more than

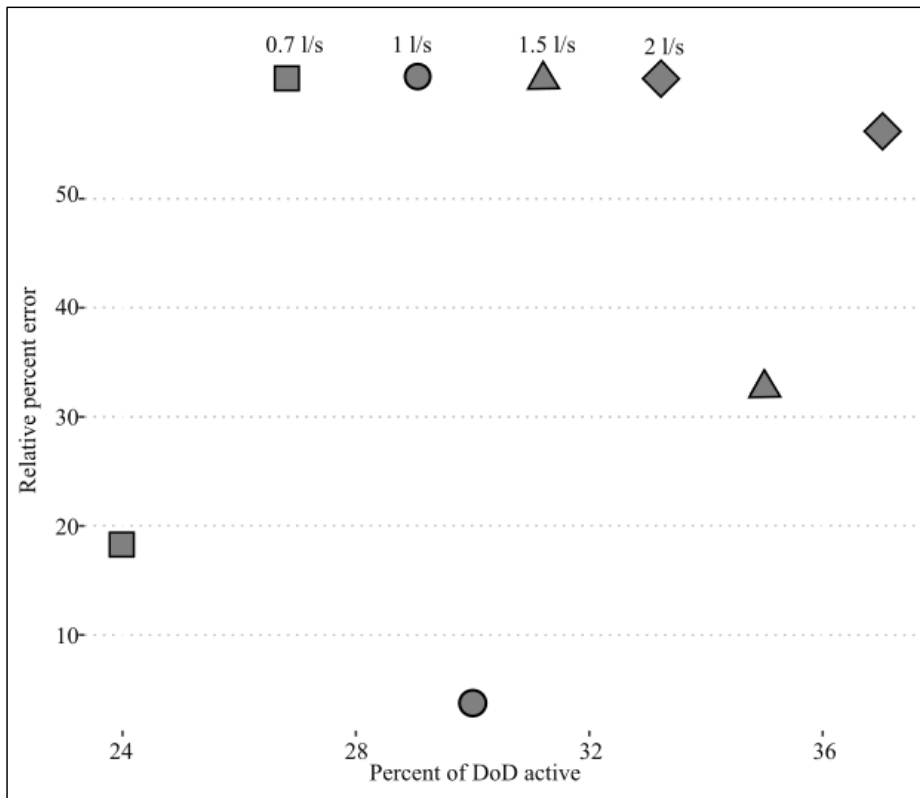
570 one morphological unit ( Liébault et al., 2012; Vázquez-Tarrío et al., 2019) and coupled with future studies, perhaps  
571 determine the conditions under which a characteristic path length is inappropriate to estimate sediment transport.

572 From the San Juan River data we see that for a year with moderate flow, as characterized by the authors, that very few  
573 tracers traveled further than the first depositional site downstream of their insertion point (McQueen et al., 2021).  
574 However, the moderate flow year for which we had corresponding tracer and DoD data resulted in two of the three sites  
575 with positively skewed distributions, and only bar six showing a mode near the bar apex, which also corresponded to  
576 the IMF 5 path length (Fig. 7). The moderate flow conditions could explain why our estimates lined up more closely  
577 with the bar apex for bar 15, where in the previous high flow year the majority of tracers were deposited resulting in a  
578 symmetrical distribution (Fig. 8 from McQueen et al., 2021). It could be that our method is strongly influenced by the  
579 morphology of the channel such that when flow is insufficient to create symmetrical or bi modal path length  
580 distributions, we overestimate by using the characteristic path length because the majority of particles are not reaching  
581 the next major depositional site downstream (i.e., a positively skewed distribution). Additionally, when the flow  
582 exceeds a yet unidentified threshold, the majority of particles move more than one depositional site downstream and  
583 therefore we underestimate sediment transport by using the characteristic path length. We can speculate that this is  
584 happening to some extent in the flume experiment. We see that at the lowest discharge, 0.7 l/s, we slightly overestimate  
585 the sediment flux especially using IMF 5 (Fig. 6) and underestimate the flux at the highest discharge, 2 l/s, where we  
586 also see a simplification of channel morphology (Fig. 6, 3). Because we did not have tracers in the flumes we can not  
587 say if the path length distributions were in fact different between the lowest and highest discharges. Future applications  
588 of this method with tracer data both in the flumes and in the field could help to understand when the characteristic  
589 length scale of morphology extracted by the method is an appropriate estimate of sediment transport and if this  
590 corresponds to flow metrics and path length distributions. In the flume studies we tested the idea that the majority of  
591 particles are bypassing the first depositional site simply by doubling the estimated path length. Assuming that sediment  
592 is not trapped in the first depositional area but in the second one and doubling the path length we more closely estimate  
593 the sediment transport at the higher discharges (i.e., estimates are not significantly different than the measured averages  
594 ( $p > 0.05$ ) but overestimate the sediment transport at the 0.7 l/s and 1 l/s discharges ( $p < 0.05$ ) (Fig. A5).

### 595 **5.1.2 Confinement**

596 It is possible that due to the confined condition of the flumes, channel width may exert an outsized effect on the average  
597 bedload transport distance as the channel is unable to widen in response to an increase in discharge, therefore causing a  
598 flushing effect. In the flume experiment, we found that the VMD-HD method performed better at the lower discharges  
599 of 0.7 l/s and 1 l/s but significantly underestimated the sediment transport at the 1.5 l/s and 2 l/s discharges (Fig. 6). The  
600 underestimation at higher discharges could be related to the amount of morphological change relative to the sediment  
601 transport. Recently, Booker and Eaton (2022) quantitatively explored the link between sediment transport and  
602 morphology and proposed an index to represent the intuitive notion that as sediment transport increases relative to  
603 morphological change, the processes become decoupled and inferences from one to another become more difficult.  
604 They developed a ‘throughput index’ which is the ratio between sediment flux and morphological change and  
605 represents how much sediment moves through a reach without leaving a topographic signature of equal magnitude.  
606 Therefore, the ratio represents how well the flux is represented morphologically with the ratio approaching 1 when all  
607 of the flux is shown as morphological change and exceeding 1 when there is transport without equivalent morphological  
608 change. In our case the flume experiments were confined, therefore, as discharge increased the channel was not able to  
609 widen and deform laterally potentially causing the sediment to move through the flume without leaving an equivalent

610 topographic signature. To explore the applicability of the method proposed we calculated the morphological active  
 611 width by counting the percentage of pixels in the DoD that showed topographic change after filtering (we applied this  
 612 metric only for the flume experiments since the San Juan River DoDs do not include the submerged part of the  
 613 channel). The morphological active width increased with discharge as expected and was positively correlated with the  
 614 error of our estimates (Fig. 8). This result exposes a limitation of the morphological method in general and our  
 615 application specifically, that is, confined channels with high transport relative to morphological change are likely poor  
 616 candidates for the morphological method as inferences between changes in morphology and sediment transport become  
 617 decoupled. Further applications of this method in the field and in the lab could identify a potential threshold defined by  
 618 the throughput index (Booker and Eaton, 2022) or the morphological active width described in this study. The  
 619 advantage of using the morphological active width as opposed to the throughput index is that it can be determined from  
 620 the DoD without direct sediment transport measurements.



621  
 622 **Figure 8: Relative percent error between estimated flux using the VMD-HD method and the measured flux in the**  
 623 **flume experiments (y-axis) vs the percentage of the DoD showing morphological change (x-axis). Different**  
 624 **discharges are denoted by shape.** discharges under the flume conditions. It is possible that at higher discharges the  
 625 characteristic path length is not equal to the spacing of erosion and deposition because the particles are moving farther  
 626 than the next depositional site downstream. For instance, if we double the estimated path length, hypothesizing a  
 627 sediment is not trapped in the first depositional area but in the second one, we more closely estimate the sediment

transport at the higher discharges (i.e., estimates are not significantly different than the measured averages ( $p > 0.05$ ) but overestimate the sediment transport at the 0.7 l/s and 1 l/s discharges ( $p < 0.05$ ) (Appendix Fig.

### 5.1.3 Morphological controls

Previous studies have shown that in gravel bed rivers, macroform spacing is typically 5-7 channel widths (Montgomery and Buffington, 1997) and therefore half of that spacing, i.e. pool to bar, may be considered a proxy for the characteristic path length. We compared our estimates of path length to (half) of both 5 and 7 times the channel width in the flumes and found that the IMF 5 estimates of path length were between the 5 and 7 channel widths for all but the highest discharge (Fig. A6). Interestingly, the manually measured distances were less than the 5-7 channel widths for all discharges but approaching 5 channel widths at the 2 l/s discharge (Fig. A6). When used to calculate sediment flux, the estimates derived from using 5 and 7 channel widths were not significantly different than our VMD-HD estimates at discharges 0.7-1.5 l/s or the measured flux at all discharges (Fig. A5). Here we are likely seeing a good correspondence between the characteristic path length, width, and sediment transport, because at formative discharges, morphology is the primary control on bedload travel distance. Whereas at lower discharges, where the morphology is relatively stable, discharge may exert a stronger control on path length. Because we do not have tracer data in the flumes for comparison, we can only rely on the sediment transport measurements for validation (A1). A second explanation is that the actual path length does not change with the increase in discharge because the channel width and morphological unit spacing exert a stronger control than any hydrologic variable which has also been observed in previous studies (Beechie, 2001; Pyrcce and Ashmore, 2003b; Vázquez-Tarrió et al., 2019). The width may exert an outsized effect in this case because the flume is laterally confined and unable to widen in response to an increase in discharge. Because we do not have tracer data in the flumes for comparison, we can only rely on the sediment transport measurements for validation which indicate that we are underestimating the sediment transport at higher discharges, thus supporting the first explanation, but further flume studies with both sediment flux and tracer data for validation could help resolve this question. The periodicity we extract from the DoDs as an estimate of path length corresponds to previous observations of preferential particle deposition at specific morphological units and relationships to channel morphology (Beechie, 2001; Pyrcce and Ashmore, 2003a, b; Kasprak et al., 2015; McDowell and Hassan, 2020; McDowell et al., 2021). In the San Juan River study, our estimates aligned closely with the secondary modes in the particle path length distributions (Fig. 7) consistent with observations that at channel forming flows, particle path lengths tend to be bi or multimodal with secondary modes corresponding to the location of bars (Pyrcce and Ashmore, 2003b). This preliminary result should be further examined with additional field data in multi-threaded channel types.

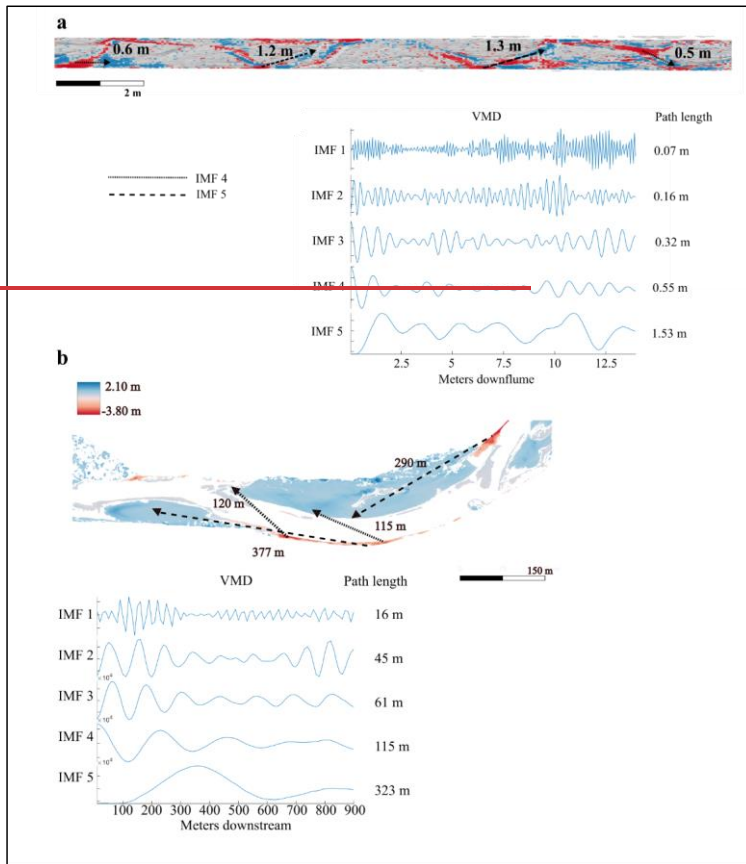
We expected that the path length in more complex channels such as braided configurations would be more difficult to estimate due to the possibility of multiple path lengths active at different flow stages. In this study both the flume experiment and the field study exhibited a wandering morphology although in the flume experiment, the channel began to simplify at higher discharges, likely due to the inability of the channel to widen in response to the increase in discharge. Further, path length estimates did not change significantly between the discharges whereas the erosion volume increases with discharge, and that, as mentioned previously, potentially contributed to the underestimation of sediment flux at the higher discharges. Additionally, at the 1.5 l/s, and 2 l/s discharges, the patches of erosion and deposition began to overlap, therefore, the wavelike pattern from areas of erosion to deposition represented by the IMF 5 vector became flattened (Fig. 3, A1). To disentangle the confounding erosion and deposition from the net vector, we applied the VMD method to a vector created from erosion and deposition separately. When calculating the path length using the erosion or deposition vectors, we took half of the resulting path length as we are still interested in the distance

668 from erosion to deposition rather than erosion to erosion. We found that the path lengths generated from these vectors  
669 were not significantly different than the path lengths generated using the net vector ( $p > 0.05$ ) (Fig. A6) nor were the  
670 estimates of sediment transport (Fig. A5) This evidence supports the use of the net vector in this case because it appears  
671 that erosion and deposition were similarly distributed. However, in rivers with differing morphology, perhaps braided  
672 systems, we might suspect that erosion will be more localized than deposition which can be dispersed (Goff and  
673 Ashmore, 1994). In these cases, using VMD to decompose the net, erosion, and deposition separately could give further  
674 insight into how deposition and erosion are contributing to the net change. For example, deposition may contribute little  
675 to net vector if the relative magnitude of the oscillations is small compared to erosion which tends to be more  
676 concentrated. In addition to estimating a characteristic path length, this decomposition could give further insight into the  
677 nature of depositional and erosional processes in a reach. We also recognize that perhaps when multiple channels are  
678 present and active, it may be beneficial to segregate the DoD, treating each channel as a separate system and generate  
679 multiple path length estimations and avoid compensating erosion and deposition within the cross section. Further  
680 investigations are needed in the lab and in the field to propose robust methodologies to assess realistic ranges of path  
681 lengths from DoD for varying river patterns.

#### 682 **5.1.4 Using the IMFs**

683 The path length-based method for calculating sediment transport necessitates that a single path length be selected and  
684 this is surely an oversimplification of reality. Encouragingly, the flume experiment shows that by using the VMD-HD  
685 method to select the path length, we are able to reasonably approximate sediment transport at the lower discharges (Fig.

686 The VMD-HD method presented here selects one of the five IMFs to be used as an estimate of path length based on the  
687 geometric similarity, as measured by the Hausdorff distance, of the IMF to the original data vector. However, we  
688 presume that not only does the method occasionally select an erroneous IMF (IMF 1 for example) but it also reasons  
689 that in some cases more than one IMF could represent the pattern of erosion and deposition in the DoD and thereby the  
690 characteristic path length. In the flume experiment, the VMD-HD method selected the longest wavelength, IMF 5, 74%  
691 of the time and IMF 4, 24% of the time. There was only one instance in which IMF 1 was selected and neither IMF 2 or  
692 3 were ever selected. Likewise, IMF 5 was selected for all three bars in the San Juan River dataset. This result agrees  
693 with observations from the signal processing literature wherein the lower frequency (in our case wavelength) IMFs (4  
694 and 5) are thought to represent the true signal whereas the higher frequency (shorter wavelength) IMFs are attributed to  
695 noise (Boudraa et al., 2005). In our case we can verify visually that IMF 5 is most likely representative of the path  
696 length by tracing the path from erosional site to depositional site within the DoD using the manual method (Fig. 3 & 8).



697

698

699

700

701

702

703

704

705

706

707

708

709

710

711

712

6). However, when applying this method to a real case study, like that of the San Juan River, it is important to consider if the results make sense given what is known about the channel and the time and magnitude of flood events between surveys, potentially taking into account both IMF 4 and IMF 5 to generate a range of plausible transport or path lengths. The VMD-HD method presented here selects one of the five IMFs to be used as an estimate of path length based on the geometric similarity, as measured by the Hausdorff distance, of the IMF to the original data vector. However, we presume that not only does the method occasionally select an erroneous IMF (IMF 1 for example where the path length is on the order of mm) but it also reasons that in some cases more than one IMF could represent the pattern of erosion and deposition in the DoD or perhaps a range due to the heterogeneous nature of sediment transport. In the flume experiment, the VMD-HD method selected the longest wavelength, IMF 5, 74% of the time and IMF 4, 24% of the time. There were only two instances in which IMF 1 was selected and neither IMF 2 or 3 were ever selected. Likewise, IMF 5 was selected for all three bars in the San Juan River dataset. This result agrees with observations from the signal processing literature wherein the lower frequency (in our case wavelength) IMFs (4 and 5) are thought to represent the true signal whereas the higher frequency (shorter wavelength) IMFs are attributed to noise (Boudraa et al., 2005). In our case we can verify visually that IMF 5 is most likely representative of the characteristic path length by tracing the path from erosional site to depositional site within the DoD using the manual method (Fig. 9). Here we see that the longest

IMF captures the spacing between erosional and depositional patches as estimated by other methods (Redolfi, 2014; Vericat et al., 2017; Calle et al., 2020). This study, as the others, supports the idea that the periodic nature of erosion and deposition can be used to estimate sediment transport and helps to clarify the conditions where this approach is valid. Moreover, this study provides an objective and repeatable method to estimate the characteristic path length.

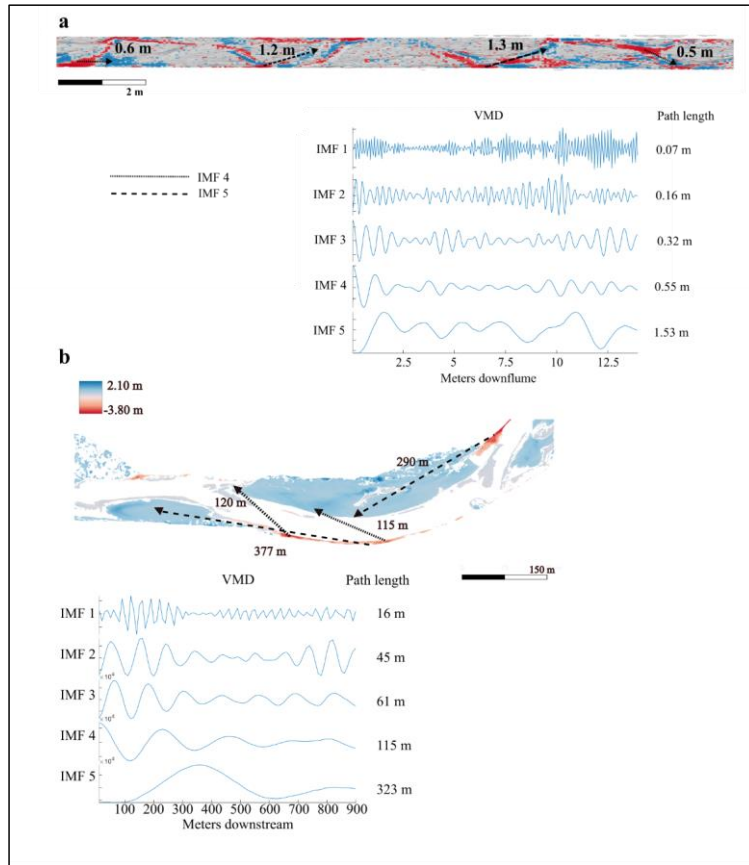


**Figure 89:** DoD with arrows showing possible path lengths between areas of erosion (red) to deposition (blue) corresponding to both IMF 4 and IMF 5. The VMD breakdown including all IMFs and the corresponding path lengths are shown for an experimental run from the 1.5 l discharge (a) and bar 15 from the San Juan River (b).

We Different IMFs also see allow us to explore multiple periodicities, such as shorter path lengths in the DoDs that may correspond to IMF 4 (Fig. 89). The method we present here to select one of the IMFs to represent the periodicity is convenient for assigning a characteristic path length to be used in sediment transport calculations. However, we recognize that in reality there is not one path length but rather a distribution. However, it is unclear if the range of IMFs may be used to estimate aspects of the path length distribution. As a first step, we see that in the San Juan River the path lengths associated with IMF 4 and IMF 5 bracket the mean, median, and key depositional areas associated with the path length distribution (Fig. 7). With future studies it may be possible to set a range of plausible transport based on IMFs 4 and 5. The path length-based method for calculating sediment transport necessitates that a single path length be selected



and this is surely an oversimplification of reality. Encouragingly, the flume experiment shows that by using the VMD-HD method to select the path length, we are able to reasonably approximate sediment transport at the lower discharges (Fig. 6) even with an occasional erroneous result (i.e., IMF 1). However, when applying this method to a real case study, like that of the San Juan River, it is important to consider if the results make sense given what is known about the channel and the time and magnitude of flood events between surveys, potentially taking into account both IMF 4 and IMF 5 to generate a range of plausible transport.

The periodicity we extract from the DoDs as an estimate of path length corresponds to previous observations of preferential particle deposition at specific morphological units and relationships to channel morphology (Beechie, 2001; Kasprak et al., 2015; Pyree and Ashmore, 2003b). In the San Juan River study, our estimates aligned closely with the secondary modes in the particle path length distributions (Fig. 7) consistent with observations that at channel forming flows, particle path lengths tend to be bi- or multimodal with secondary modes corresponding to the location of bars (Pyree and Ashmore, 2003b). This preliminary result should be further examined with additional field data in multiple channel types.

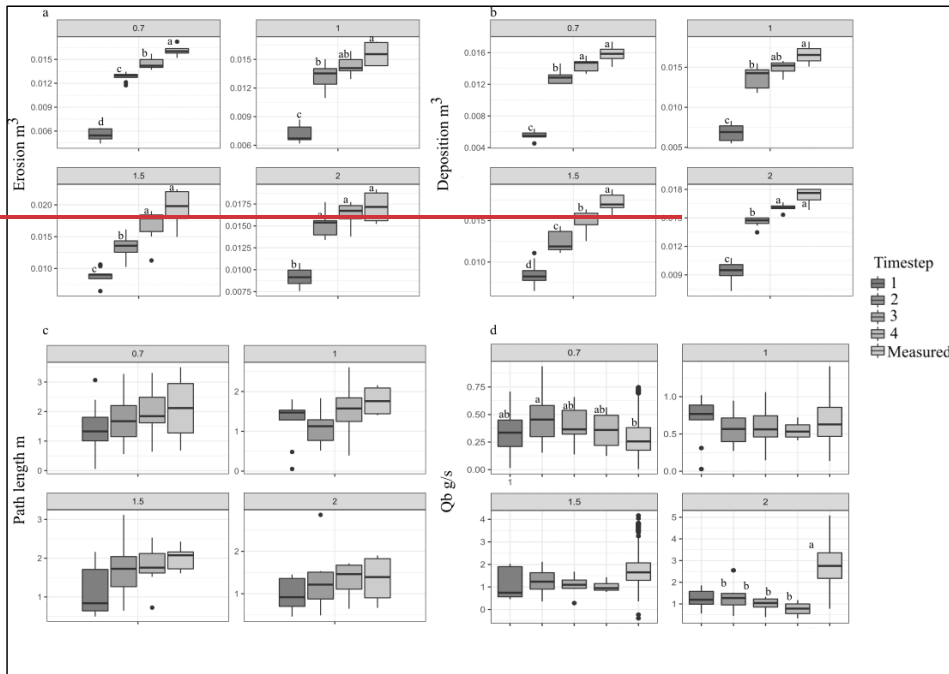
We expected that the path length in more complex channels such as braided configurations would be more difficult to estimate due to the possibility of multiple path lengths active at different flow stages. In this study both the flume experiment and the field study exhibited a wandering morphology although in the flume experiment, the channel began to simplify at higher discharges. This is likely due to the inability of the channel to widen in response to the increase in discharge. Further, path length estimates did not change significantly between the discharges whereas the erosion volume increases with discharge, and that, as mentioned previously, potentially contributed to the underestimation of sediment flux at the higher discharges. Additionally, at the 1.5 l/s, and 2 l/s discharges, the patches of erosion and deposition began to overlap, therefore, the wavelike pattern from areas of erosion to deposition represented by the IMF 5 vector became flattened (Fig. 3). Further, when multiple channels are present and active, it may be beneficial to segregate the DoD, treating each channel as a separate system and generate multiple path length estimations. Further investigations are needed in the lab and in the field to propose robust methodologies to assess realistic ranges of path lengths from DoD for varying river patterns.

## 5.2 DoD related uncertainties

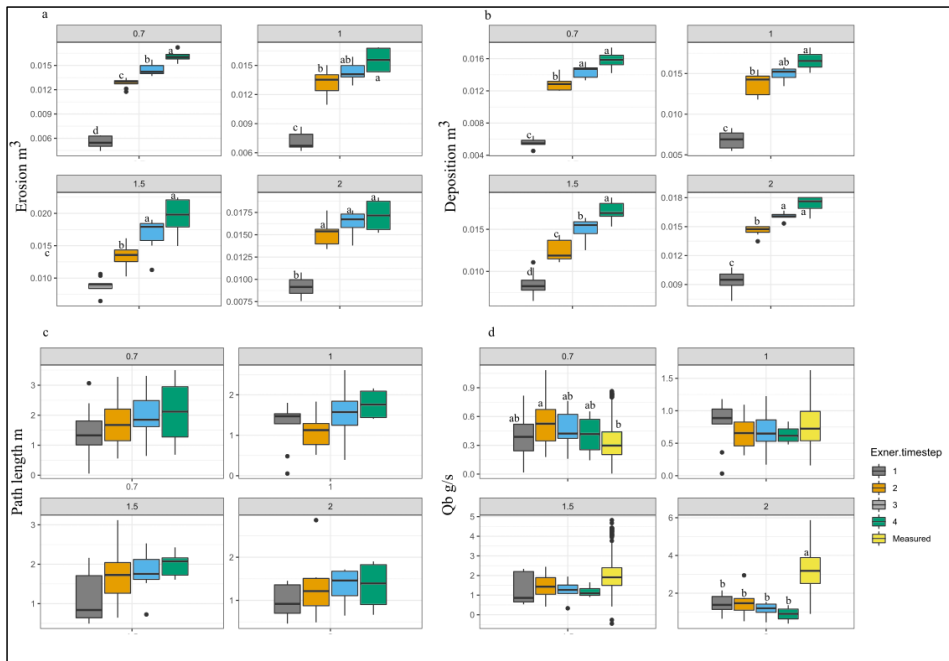
Any application of the morphological method using DoDs is sensitive to the error thresholding method used due to the way in which different thresholding techniques influence both the volumes of erosion and deposition as well as their spatial patterning (Brasington et al., 2003; Wheaton, 2008; Wheaton et al., 2010; Vericat et al., 2017). Because our method relies on the spacing between areas of erosion and deposition which is related to the size of the patches as well as which patches are detected, we considered that thresholding techniques could greatly affect the estimates of path length. We tested this hypothesis by applying the method to both the raw and filtered DoDs for the Trento flume experiment and found that while the volumes of erosion and deposition were lower after thresholding as expected ( $p < 0.001$ ), the path length estimates were not significantly different ( $p > 0.05$ ) (Appendix-Table A1). While the thresholding here did not affect the path length estimates, we might imagine a scenario in which an entire area of erosion or deposition is removed through aggressive thresholding techniques, thereby potentially affecting the path length estimates and therefore caution that appropriate thresholding is important for the application of this method and the morphological method in general. It is also important to consider the spatial resolution (i.e. raster cell size) of the DoD when applying this method. Similarly to thresholding or selecting a bin size, the spatial resolution of the DoD could cause information to be lost if the cell size is large enough to aggregate erosion and deposition within the same

769 cell (see for instance the comparison made in Antoniazza et al., 2019). We see less of a risk in using smaller cell sizes  
770 as the method already calls for aggregation in the binning process and in theory VMD should be able to separate the  
771 small scale fluctuations as short wavelength IMFs. However, this is an open question and should be evaluated by the  
772 user on a case by case basis.

773 The time between surveys is of equal importance to the path length in the estimation of virtual velocity ~~Eq. (2)~~ and in  
774 the field can be highly uncertain due to poor availability of hydrologic data and/or the uncertainty of estimating the  
775 onset of transport based on a critical shear stress. Further, as time between surveys increases, so too does the probability  
776 of compensating erosion and deposition which can affect both the volumes of erosion and deposition and the  
777 topographic signatures (Lindsay and Ashmore, 2002; Vericat et al., 2017) necessary for VMD-HD method. We tested  
778 how the time between surveys might affect both the volumes of erosion and deposition and our path length estimates by  
779 differencing DEMs not every time step but between two, three, and four timesteps, each time step being one of the nine  
780 runs in the lab of phase 3 (see method). Not surprisingly the volume of erosion and deposition increased significantly  
781 with increasing time between surveys with the largest increase between the 1<sup>st</sup> timestep and 2<sup>nd</sup> timestep (Fig. 9)-10).  
782 The path length estimates did not increase significantly for any of the discharges (Fig. 9e10c) indicating that the path  
783 length estimate is stable, likely because, as already noted, the spacing of erosion and deposition is related to the position  
784 of erosional and depositional features which do not change much in ~~a confined experiment the flume~~. When both of  
785 these parameters are used in the sediment transport calculations and normalized by the increased time between surveys,  
786 we found no statistically significant difference between the estimates (Fig. 9d10d). However, though not statistically  
787 significant, there is an apparent decreasing trend in the sediment flux with the increased time between surveys,  
788 especially for the 2 l/s discharge that may indicate compensation (Fig. 9d10d). Despite the apparent trend at the highest  
789 discharge this is a promising result in that even by increasing the time interval by a factor of 4 we are still able to  
790 estimate sediment transport reasonably at the lower discharges. In the field there are often multiple flood events of  
791 differing magnitude in the year between surveys as was the case with the San Juan River study (McQueen et al., 2021).  
792 Although there were five flood events of differing magnitudes between the San Juan River surveys, we were still able to  
793 estimate path lengths corresponding to potentially significant features of the RFID-tracer data with an error of less than  
794 30% path length distributions (Fig. 7).



795



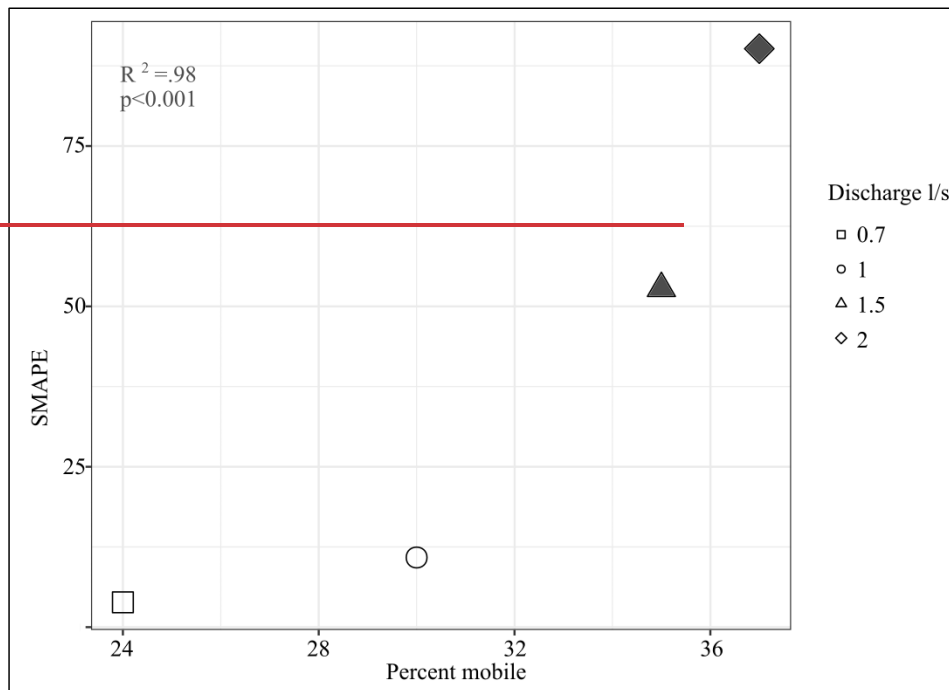
796

797 **Figure 910:** (a) Erosion measured from the flume experiments for each discharge and each timestep (b)  
 798 **deposition** (c) path length estimates using VMD-HD method (d) sediment flux estimated using VMD-HD method  
 799 **and measured. Significant post-hoc Tukey results are denoted by letters a-d ( $\alpha=0.05$ ).**

### 800 **5.3 Applicability of the method**

801 When evaluating the efficacy of our proposed method it is important to keep in mind the uncertainty of even direct  
 802 measurement of sediment transport. The spatial and temporal frequency required to overcome the noise of measurement  
 803 uncertainty (i.e., achieve an acceptable signal to noise ratio) in some cases can require sub-daily monitoring with  
 804 precise equipment (Grams et al., 2019). The variability of sediment transport measurements in the flume study ranged  
 805 from a standard deviation of approximately 30% to over 50% of the averaged flux (Fig. 3). Given this high variability,  
 806 our reach scale averages were not significantly different from the measured averages for the 0.7 l/s and 1 l/s discharges  
 807 (Fig. 6). Further, our method produced path length estimates which correspond to the distance between erosional and  
 808 depositional sites on the DoD in both the flumes and field (Fig. 7).

809 In the flume experiment, we found that the VMD-HD method performed better at the lower discharges of 0.7 l/s and 1  
 810 l/s but significantly underestimated the sediment transport at the 1.5 l/s and 2 l/s discharges (Fig. 6). In Sect. 5.1 we  
 811 discussed that this underestimation is likely due to our limitations in the deriving realistic path lengths from DoDs. The  
 812 underestimation at higher discharges could be related to the amount of morphological change relative to the sediment  
 813 transport. Recently, Booker and Eaton (2022) quantitatively explored the link between sediment transport and  
 814 morphology and proposed an index to represent the intuitive notion that as sediment transport increases relative to  
 815 morphological change, the processes become decoupled and inferences from one to another become more difficult.  
 816 They developed a 'throughput index' which is the ratio between sediment flux and morphological change and  
 817 represents how much sediment moves through a reach without leaving a topographic signature of equal magnitude.  
 818 Therefore, the ratio represents how well the flux is represented morphologically with the ratio approaching 1 when all  
 819 of the flux is shown as morphological change and exceeding 1 when there is transport without equivalent morphological  
 820 change. In our case the flume experiments were confined, therefore, as discharge increased the channel was not able to  
 821 widen and deform laterally potentially causing the sediment to move through the flume without leaving an equivalent  
 822 topographic signature. To explore the applicability of the method proposed we calculated the morphological active  
 823 width by counting the percentage of pixels in the DoD that showed topographic change after filtering (we applied this  
 824 metric only for the flume experiments since the San Jose DoDs do not include the submerged part of the channel). The  
 825 morphological active width increased with discharge as expected and was positively correlated with the error of our  
 826 estimates (Fig. 10). We found a strong exponential relationship between the percent of the flume that was active and the  
 827 error of our estimates ( $R^2=0.98$ ,  $p<0.01$ ) (Fig. 10). This result exposes a limitation of the morphological method in  
 828 general and our application specifically, that is, confined channels with high transport relative to morphological change  
 829 are likely poor candidates for the morphological method as inferences between changes in morphology and sediment  
 830 transport become decoupled. Further applications of this method in the field and in the lab could identify a potential  
 831 threshold defined by the throughput index (Booker and Eaton, 2022) or the morphological active width described in this  
 832 study. The advantage of using the morphological active width as opposed to the throughput index is that it can be  
 833 determined from the DoD without direct sediment transport measurements.



834  
835 **Figure 10: Symmetrical mean absolute percent error (SMAPE) between estimated and measured flux in the**  
836 **flume experiments vs the percentage of the DoD showing morphological change. Different discharges are**  
837 **denoted by shape. Filled shapes are where the sediment transport was significantly underestimated ( $\alpha=0.05$ ).  $R^2$**   
838 **and p value from exponential regression is shown.**

## 839 6 Conclusion

840 The feasibility of estimating sediment flux using the morphological method has increased dramatically with the advent  
841 of high resolution topography but has thus far been limited by the high labor demand of acquiring estimates of path  
842 length or the uncertainty of defining zero or known flux boundary. Given the observed connections between  
843 morphology and path length at channel forming flows, we hypothesized/proposed that the periodic nature of the pattern  
844 of erosion and deposition can be a proxy for particle characteristic path length in gravel bed rivers. We applied tools  
845 from signal processing to quantify this periodicity and found that our method provides estimates path length within 30%  
846 of measured tracer data by the longest wavelengths from the decomposition, IMF 4 and corresponds to the spacing of  
847 erosion and deposition visible on the DoD. Further, our method provides estimates of IMF 5 may represent meaningful  
848 bedload transport processes and IMF 5 in particular may represent the characteristic path length. We found that the path  
849 length estimates generated by IMFs 4 and 5 bracket a significant portion of measured path length coherent with channel  
850 morphology and previous observations of preferential particle deposition at given channel distributions in the field and  
851 correspond to important morphological units, specifically bar heads and margins. When, in the flume experiment we  
852 found that IMF 4 and 5 path lengths also bracket the manually measured distances between erosional and depositional  
853 patches and when extended to calculate sediment flux our estimates were not significantly different from the measured  
854 average at low discharges. Importantly we found that an insensitivity of the method to increasing discharge and propose  
855 that perhaps limits arise where discharge increases in confined channels/settings, such as in the flume, and sediment

transport becomes decoupled from morphological changes. Our method provides a reasonable estimation of path length based solely on remotely sensed data and new view of the periodic nature of erosion and deposition in sediment transport and a novel methodology to estimate/extract sediment fluxes associated with specific channel morphological processes through DoD interpretation/transport information using only DoDs.

## Appendix A

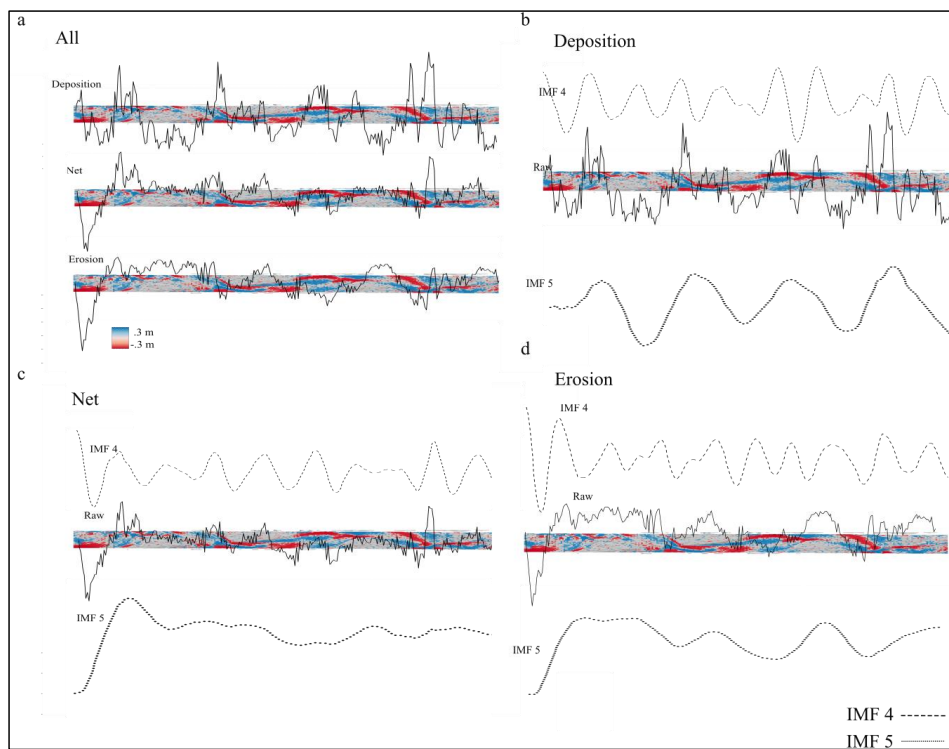
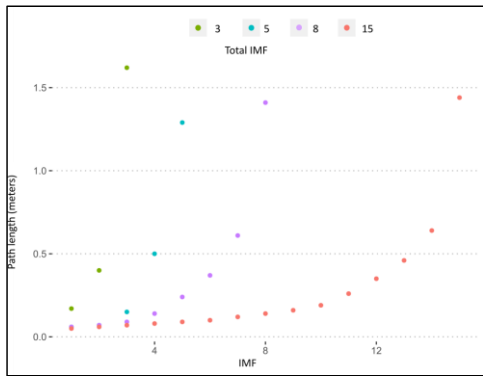


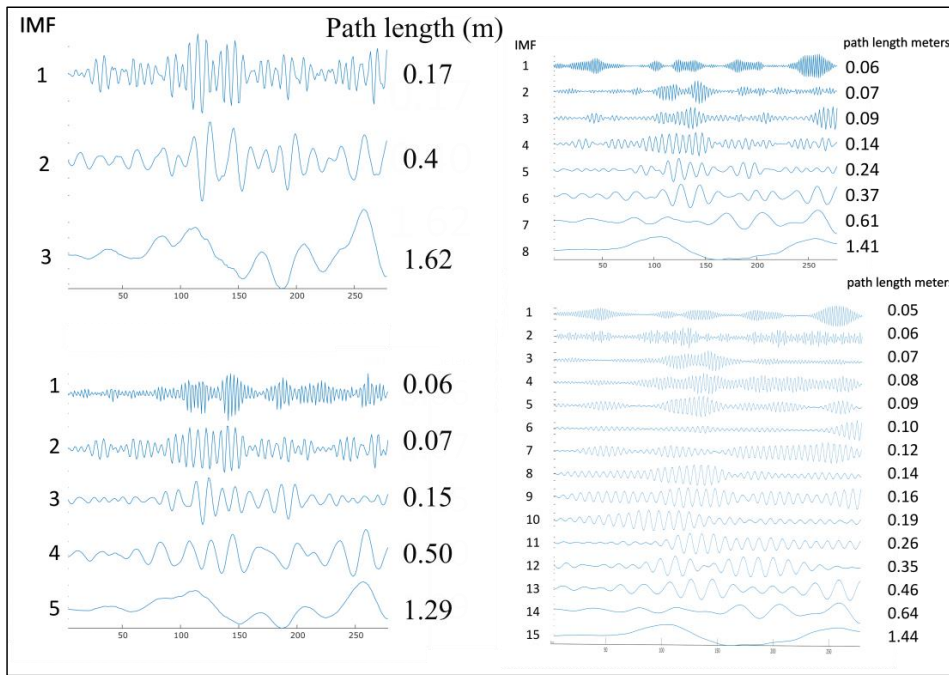
Figure A1. DoDs from the 2 l/s discharge. a) Vector of deposition, erosion, and the net. b) Raw depositional vector and the decomposition of IMF 4 and IMF 5 from that depositional vector. c) Net vector and the decomposition of IMF 4 and IMF 5 from that net vector. d) Raw erosional vector and the decomposition of IMF 4 and IMF 5 from that erosional vector.



870

871

Figure A2. Path length estimates using a maximum of 3,5,8, or 15 IMFs.

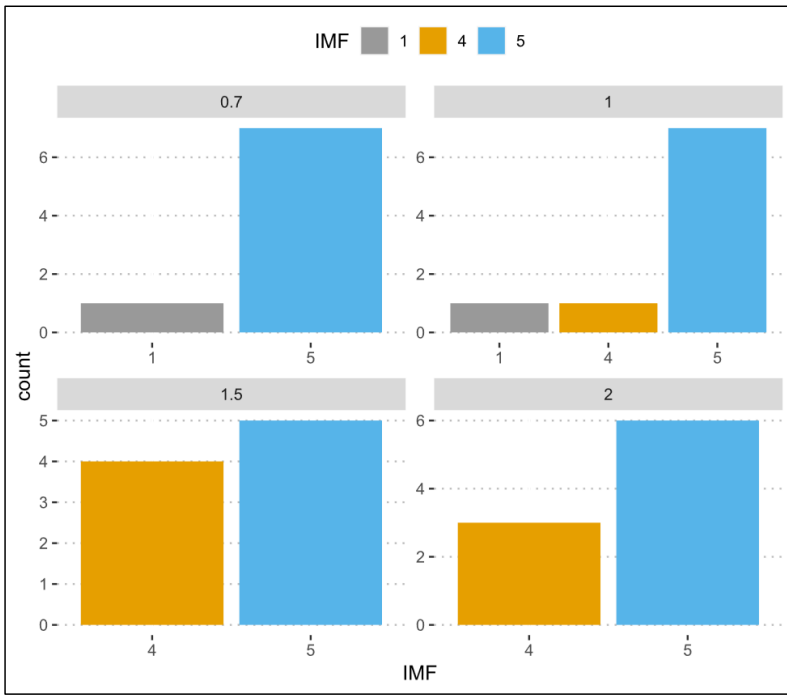


872

873

874

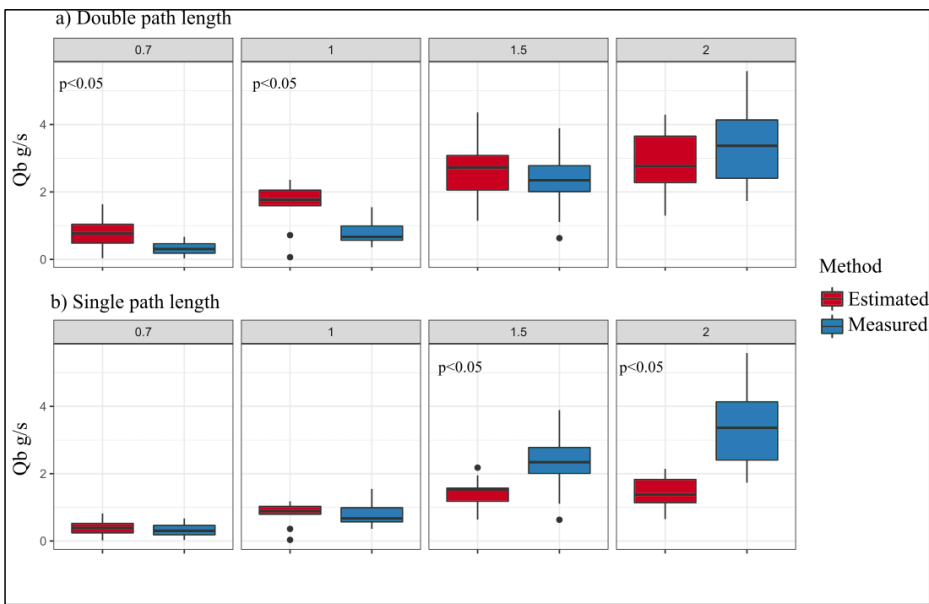
Figure A3. Path length estimates from VMD for 1.5 l/s discharge. Sensitivity of maximum number of IMFs.



875

876

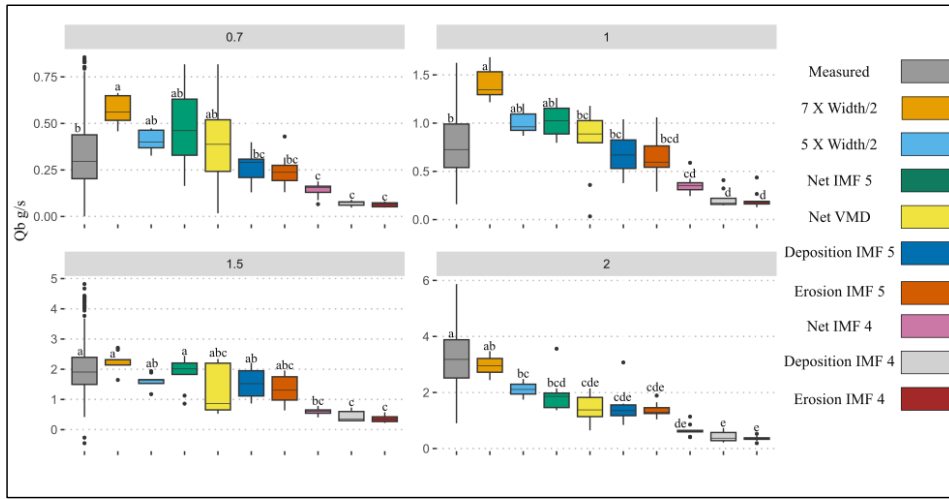
Figure A4. Number of times each IMF was selected by the VMD-HD method for each discharge.



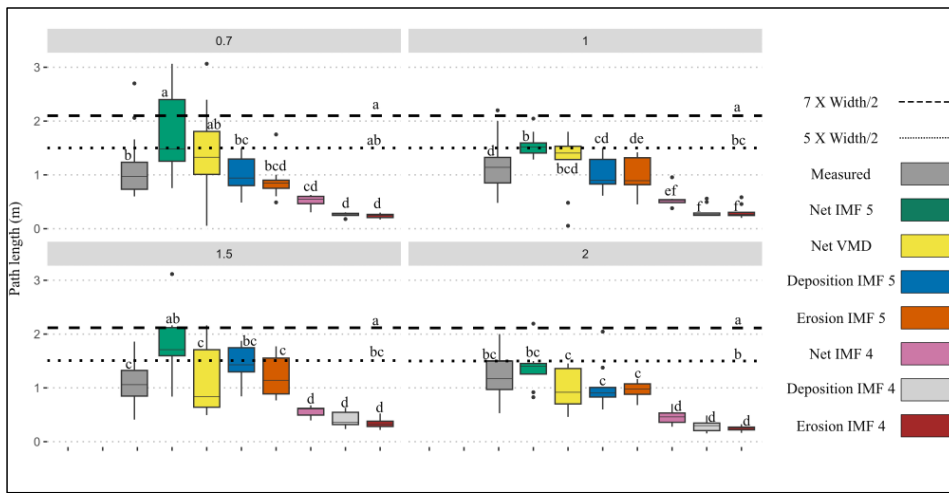
877



878 Figure A5. Sediment transport calculated using the single path length estimate from the VMD-HD method (b) and  
 879 doubling the path length estimate (a). Estimated flux is red and measured flux is blue. Significant p values are shown.  
 880



881  
 882 Figure A6. Sediment transport (g/s) calculated using channel dimensions, IMFs 4 and 5 for net, erosion, and deposition  
 883 vectors. Compared to the measured flux for each discharge. Post hoc Tukey results denoted by letters a-f.



884  
 885 Figure A7. Path length estimates from the channel dimensions, IMFs 4 and 5 for net, erosion, and deposition  
 886 vectors compared to manually measured distances for each discharge. Post hoc Tukey results denoted by letters a-f.  
 887

Table 1A.1. Results from filtered vs raw DoDs from the flume experiments.

Discharge	Path length raw (m)	Path length filtered (m)	Qb estimated raw(g/s)	Qb estimated filtered (g/s)	Erosion raw (m3)	Deposition raw(m3)	Erosion filtered (m3)	Deposition filtered (m3)
0.7								
1								
1.5								
2								

Formatted: Caption1



<u>2</u>	<u>0.71</u>	<u>0.66</u>	<u>1.30</u>	<u>0.74</u>	<u>0.01</u>	<u>0.01</u>	<u>0.01</u>	<u>0.01</u>
Summary								
Discharge	Erosion	Deposition	Path Length	Qb				
0.7	p<0.001**	p<0.001**	p>0.05	p<0.05*				
1	p<0.001**	p<0.001**	p>0.05	p<0.05*				
<u>2</u>	p<0.001**	p<0.001**	p>0.05	p>0.05*				
<u>2</u>	<u>p&lt;0.001**</u>	<u>p&lt;0.001**</u>	<u>p&gt;0.05</u>	<u>p&gt;0.05</u>				
*p-values from student's t test between raw and filtered data								

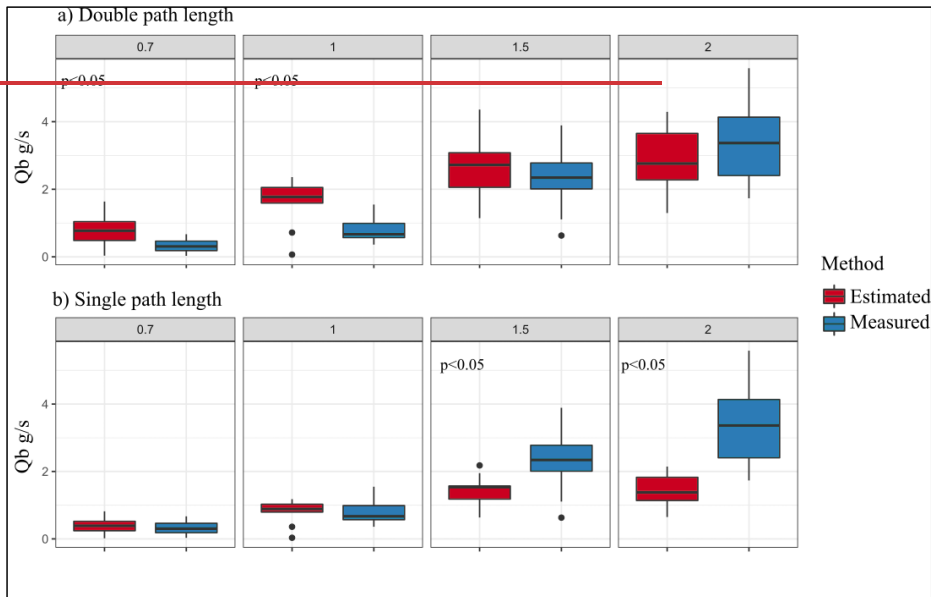


Figure 1A. Sediment transport calculated using the single path length estimate from the VMD-HD method (b) and doubling the path length estimate (a). Estimated flux is red and measured flux is blue. Significant p values are shown.

Code

#### Data availability

Data and code are available upon request from the corresponding author at <https://doi.org/10.5281/zenodo.8014453>.

#### Author contribution

LC, SB, WB and NS conceptualized the study. EP and WB performed the experiments. LC, SB and WB designed the method. LC performed statistical analysis. LC, EP, and WB wrote the manuscript. LC, SB, EP, WB, and NS edited the manuscript.

#### Competing interests

The authors declare they have no competing interests.

Formatted: Caption1

Formatted Table

Deleted Cells

Formatted: Caption1

Formatted: Caption1

Formatted: Caption1

Formatted: Caption1

Formatted: Caption1

Formatted: Caption1

Formatted Table

Deleted Cells

900 **Financial support**

901 This work was supported by the CARIPARO foundation and the University of Padova.

902 **References**

- 903 [Ashmore, P.E., Church, M.: Sediment transport and river morphology: a paradigm for study. Gravel-bed Rivers in the](#)  
904 [Environment, Hey, R.D., Bathurst, J.C., Thorne, C.R. \(eds\). Wiley: Chichester, 115–148, 1998.](#)
- 905 [Antoniazza, G., Bakker, M., and Lane, S. N.: Revisiting the morphological method in two-dimensions to quantify bed-](#)  
906 [material transport in braided rivers. Earth Surf. Process. Landf., 44, 2251–2267. <https://doi.org/10.1002/esp.4633>, 2019.](#)
- 907 [Ashmore, P. E. and Church, M.: Sediment transport and river morphology: a paradigm for study. Gravel-Bed Rivers](#)  
908 [Environ., 345, 115–139, 1998.](#)
- 909 [Bakker, M., Antoniazza, G., Odermatt, E., and Lane, S. N.: Morphological Response of an Alpine Braided Reach to](#)  
910 [Sediment-Laden Flow Events. J. Geophys. Res. Earth Surf., 124, 1310–1328, <https://doi.org/10.1029/2018JF004811>,](#)  
911 [2019.](#)
- 912 [Barnhart, B. L. and Eichinger, W. E.: Empirical Mode Decomposition applied to solar irradiance, global temperature,](#)  
913 [sunspot number, and CO2 concentration data. J. Atmospheric Sol.-Terr. Phys., 73, 1771–1779,](#)  
914 [https://doi.org/10.1016/j.jastp.2011.04.012, 2011.](#)
- 915 Beechie, T. J.: Empirical predictors of annual bed load travel distance, and implications for salmonid habitat restoration  
916 and protection, Earth Surf. Process. Landf., 26, 1025–1034, <https://doi.org/10.1002/esp.251>, 2001.
- 917 Booker, W. H. and Eaton, B. C.: Morphodynamic styles: characterising the behaviour of gravel-bed rivers using a  
918 novel, quantitative index, Earth Surf. Dyn., 10, 247–260, <https://doi.org/10.5194/esurf-10-247-2022>, 2022.
- 919 Boudraa, A.-O., Cexus, J.-C., and Saidi, Z.: EMD-Based Signal Noise Reduction, Signal Process., 1, 2005.
- 920 [Brasington, J., Rumsby, B. T., and McVey, R. A.: Monitoring and modelling morphological change in a braided gravel-](#)  
921 [bed river using high resolution GPS-based survey. Earth Surf. Process. Landf., 25, 973–990,](#)  
922 [https://doi.org/10.1002/1096-9837\(200008\)25:9<973::AID-ESP111>3.0.CO;2-Y, 2000.](#)
- 923 [Brasington, J., Langham, J., and Rumsby, B.: Methodological sensitivity of morphometric estimates of coarse fluvial](#)  
924 [sediment transport, Geomorphology, 53, 299–316, \[https://doi.org/10.1016/S0169-555X\\(02\\)00320-3\]\(https://doi.org/10.1016/S0169-555X\(02\)00320-3\), 2003.](#)
- 925 [Brenna, A. and Surian, N.: Coarse sediment mobility and fluxes in wide mountain streams: Insights using the virtual](#)  
926 [velocity approach. Geomorphology, 427, 108625, <https://doi.org/10.1016/j.geomorph.2023.108625>, 2023.](#)
- 927 [Brenna, A., Surian, N., and Mao, L.: Virtual Velocity Approach for Estimating Bed Material Transport in Gravel-Bed](#)  
928 [Rivers: Key Factors and Significance, Water Resour. Res., 55, 1651–1674, <https://doi.org/10.1029/2018WR023556>,](#)  
929 [2019.](#)
- 930 [Brenna, A., Surian, N., Ghinassi, M., and Marchi, L.: Sediment–water flows in mountain streams: Recognition and](#)  
931 [classification based on field evidence. Geomorphology, 371, 107413, <https://doi.org/10.1016/j.geomorph.2020.107413>,](#)  
932 [2020.](#)
- 933 [Brewer, P. A. and Passmore, D. G.: Sediment budgeting techniques in gravel-bed rivers. Geol. Soc. Lond. Spec. Publ.,](#)  
934 [191, 97–113, <https://doi.org/10.1144/GSL.SP.2002.191.01.07>, 2002.](#)
- 935 [Calle, M., Calle, J., Alho, P., and Benito, G.: Inferring sediment transfers and functional connectivity of rivers from](#)  
936 [repeat topographic surveys. Earth Surf. Process. Landf., 45, 681–693, <https://doi.org/10.1002/esp.4765>, 2020.](#)
- 937 [Church, M.: Bed Material Transport and the Morphology of Alluvial River Channels. Annu. Rev. Earth Planet. Sci., 34,](#)  
938 [325–354, <https://doi.org/10.1146/annurev.earth.33.092203.122721>, 2006.](#)
- 939 Dragomiretskiy, K. and Zosso, D.: Variational Mode Decomposition, IEEE Trans. Signal Process., 62, 531–544,  
940 <https://doi.org/10.1109/TSP.2013.2288675>, 2014.
- 941 [Ferguson, R. I. and Ashworth, P. J.: Spatial patterns of bedload transport and channel change in braided and near-](#)  
942 [braided rivers. Dyn. Gravel-Bed Rivers Billi P Hey RD Thorne CR Tacconi P Eds, 1992.](#)

- 943 Garcia Lugo, G. A., Bertoldi, W., Henshaw, A. J., and Gurnell, A. M.: The effect of lateral confinement on gravel bed  
944 river morphology, *Water Resour. Res.*, 51, 7145–7158, <https://doi.org/10.1002/2015WR017081>, 2015.
- 945 [Goff, J. R. and Ashmore, P.: Gravel transport and morphological change in braided sunwapta river, Alberta, Canada,](#)  
946 [Earth Surf. Process. Landf., 19, 195–212, <https://doi.org/10.1002/esp.3290190302>, 1994.](#)
- 947 Grams, P. E., Topping, D. J., Schmidt, J. C., Hazel Jr., J. E., and Kaplinski, M.: Linking morphodynamic response with  
948 sediment mass balance on the Colorado River in Marble Canyon: Issues of scale, geomorphic setting, and sampling  
949 design, *J. Geophys. Res. Earth Surf.*, 118, 361–381, <https://doi.org/10.1002/jgrf.20050>, 2013.
- 950 Grams, P. E., Buscombe, D., Topping, D. J., Kaplinski, M., and Hazel, J. E.: How many measurements are required to  
951 construct an accurate sand budget in a large river? Insights from analyses of signal and noise, *Earth Surf. Process.*  
952 *Landf.*, 44, 160–178, <https://doi.org/10.1002/esp.4489>, 2019.
- 953 Hassan, M. A. and Bradley, D. N.: Geomorphic Controls on Tracer Particle Dispersion in Gravel-Bed Rivers, in:  
954 *Gravel-Bed Rivers*, John Wiley & Sons, Ltd, 159–184, <https://doi.org/10.1002/9781118971437.ch6>, 2017.
- 955 Hassan, M. A., Church, M., and Schick, A. P.: Distance of movement of coarse particles in gravel bed streams, *Water*  
956 *Resour. Res.*, 27, 503–511, <https://doi.org/10.1029/90WR02762>, 1991.
- 957 [Hoey, T.: Temporal variations in bedload transport rates](#)[Hassan, M. A., Church, M., and sediment storage](#)[Ashworth, P.](#)  
958 [J.: Virtual rate and mean distance of travel of individual clasts in gravel-bed rivers,](#) *Prog. Phys. Geogr. channels, Earth*  
959 *Environ.*, 16, 319–338 *Surf. Process. Landf.*, 17, 617–627,  
960 <https://doi.org/10.1177/0309133392016003031002/esp.3290170607>, 1992.
- 961 Huang, N., Chen, H., Cai, G., Fang, L., and Wang, Y.: Mechanical Fault Diagnosis of High Voltage Circuit Breakers  
962 Based on Variational Mode Decomposition and Multi-Layer Classifier, *Sensors*, 16, 1887,  
963 <https://doi.org/10.3390/s16111887>, 2016.
- 964 [Hundey, E. J. and Ashmore, P. E.: Length scale of braided river morphology: Length Scale of Braided River](#)  
965 [Morphology,](#) *Water Resour. Res.*, 45, <https://doi.org/10.1029/2008WR007521>, 2009.
- 966 Kasprak, A., Wheaton, J. M., Ashmore, P. E., Hensleigh, J. W., and Peirce, S.: The relationship between particle travel  
967 distance and channel morphology: results from physical models of braided rivers., *J. Geophys. Res. Earth Surf.*, 120,  
968 55–74, 2015.
- 969 [Lane, S. N., Richards, K. S., and Chandler, J. H.: Morphological Estimation of the Time-Integrated Bed Load Transport](#)  
970 [Rate,](#) *Water Resour. Res.*, 31, 761–772, <https://doi.org/10.1029/94WR01726>, 1995.
- 971 [Lane, S. N., Westaway, R. M., and Murray Hicks, D.: Estimation of erosion and deposition volumes in a large, gravel-](#)  
972 [bed, braided river using synoptic remote sensing,](#) *Earth Surf. Process. Landf.*, 28, 249–271,  
973 <https://doi.org/10.1002/esp.483>, 2003.
- 974 Liébault, F., Bellot, H., Chapuis, M., Klotz, S., and Deschâtres, M.: Bedload tracing in a high-sediment-load mountain  
975 stream: [Bedload tracing in a high-sediment-load mountain stream,](#) *Earth Surf. Process. Landf.*, 37, 385–399,  
976 <https://doi.org/10.1002/esp.2245>, 2012.
- 977 Lindsay, J. B. and Ashmore, P. E.: The effects of survey frequency on estimates of scour and fill in a braided river  
978 model, *Earth Surf. Process. Landf.*, 27, 27–43, <https://doi.org/10.1002/esp.282>, 2002.
- 979 [Liu, S., He, Q., Gao, R. X., and Freedson, P.: Empirical mode decomposition applied to tissue artifact removal from](#)  
980 [respiratory signal, in: 2008 30th Annual International Conference of the IEEE Engineering in Medicine and Biology](#)  
981 [Society, 2008 30th Annual International Conference of the IEEE Engineering in Medicine and Biology Society, 3624–](#)  
982 [3627,](#) <https://doi.org/10.1109/IEMBS.2008.4649991>, 2008.
- 983 Ma, W., Yin, S., Jiang, C., and Zhang, Y.: Variational mode decomposition denoising combined with the Hausdorff  
984 distance, *Rev. Sci. Instrum.*, 88, 035109, <https://doi.org/10.1063/1.4978029>, 2017.
- 985 [Mao, L., Picco, L., Lenzi, M. A., and Surian, N.: Bed material transport estimate in large gravel-bed rivers using the](#)  
986 [virtual velocity approach: Virtual velocity for bed material transport estimate,](#) *Earth Surf. Process. Landf.*, 42, 595–611,  
987 <https://doi.org/10.1002/esp.4000>, 2017.

- 988 McDowell, C. and Hassan, M. A.: The influence of channel morphology on bedload path lengths: Insights from a  
989 survival process model, *Earth Surf. Process. Landf.*, 45, 2982–2997, <https://doi.org/10.1002/esp.4946>, 2020.
- 990 McDowell, C., Gaeuman, D., and Hassan, M. A.: Linkages between bedload displacements and topographic change,  
991 *Earth Surf. Process. Landf.*, 46, 3127–3142, <https://doi.org/10.1002/esp.5221>, 2021.
- 992 McLean, D. G. and Church, M.: Sediment transport along lower Fraser River: 2. Estimates based on the long-term  
993 gravel budget, *Water Resour. Res.*, 35, 2549–2559, <https://doi.org/10.1029/1999WR900102>, 1999.
- 994 McQueen, R., Ashmore, P., Millard, T., and Goeller, N.: Bed Particle Displacements and Morphological Development  
995 in a Wandering Gravel-Bed River, *Water Resour. Res.*, 57, <https://doi.org/10.1029/2020WR027850>, 2021.
- 996 [Montgomery, D. R. and Buffington, J. M.: Channel-reach morphology in mountain drainage basins, \*GSA Bull.\*, 109,  
997 596–611, \[https://doi.org/10.1130/0016-7606\\(1997\\)109<0596:CRMIMD>2.3.CO;2\]\(https://doi.org/10.1130/0016-7606\(1997\)109<0596:CRMIMD>2.3.CO;2\), 1997.](#)
- 998 Pyrcce, R. and Ashmore, P.: The relation between particle path length distributions and channel morphology in gravel-  
999 bed streams: A synthesis, *Geomorphology*, 56, 167–187, [https://doi.org/10.1016/S0169-555X\(03\)00077-1](https://doi.org/10.1016/S0169-555X(03)00077-1), 2003a.
- 1000 Pyrcce, R. S. and Ashmore, P. E.: Particle path length distributions in meandering gravel-bed streams: results from  
1001 physical models, *Earth Surf. Process. Landf.*, 28, 951–966, <https://doi.org/10.1002/esp.498>, 2003b.
- 1002 [Pyrcce, R. S. and Ashmore, P. E.: Bedload path length and point bar development in gravel-bed river models,  
1003 \*Sedimentology\*, 52, 839–857, <https://doi.org/10.1111/j.1365-3091.2005.00714.x>, 2005.](#)
- 1004 [Redolfi, M.: \*Sediment transport and morphology of braided rivers: steady and unsteady regime\*, n.d.](#)
- 1005 Roux, C., Alber, A., Bertrand, M., Vaudor, L., and Piégay, H.: “FluvialCorridor”: A new ArcGIS toolbox package for  
1006 multiscale riverscape exploration, *Geomorphology*, 242, 29–37, <https://doi.org/10.1016/j.geomorph.2014.04.018>, 2015.
- 1007 [Schneider, J. M., Turowski, J. M., Rickenmann, D., Hegglin, R., Arrigo, S., Mao, L., and Kirchner, J. W.: Scaling  
1008 relationships between bed load volumes, transport distances, and stream power in steep mountain channels, \*J. Geophys.  
1009 Res. Earth Surf.\*, 119, 533–549, <https://doi.org/10.1002/2013JF002874>, 2014.](#)
- 1010 [Sigmund, M.: \*Voice Recognition by Computer\*, Tectum Verlag DE, 114 pp., 2003.](#)
- 1011 Upadhyay, A. and Pachori, R. B.: Instantaneous voiced/non-voiced detection in speech signals based on variational  
1012 mode decomposition, *J. Frankl. Inst.*, 352, 2679–2707, <https://doi.org/10.1016/j.jfranklin.2015.04.001>, 2015.
- 1013 [Vázquez-Tarrío, D. and Batalla, R. J.: \*Assessing Controls on the Displacement of Tracers in Gravel-Bed Rivers\*, \*Water\*,  
1014 11, 1598, <https://doi.org/10.3390/w11081598>, 2019.](#)
- 1015 [Vázquez-Tarrío, D., Recking, A., Liébault, F., Tal, M., and Menéndez-Duarte, R.: Particle transport in gravel-bed  
1016 rivers: Revisiting passive tracer data: Particle transport in gravel-bed rivers, \*Earth Surf. Process. Landf.\*, 44, 112–128,  
1017 <https://doi.org/10.1002/esp.4484>, 2019.](#)
- 1018 [Vericat, D., Church, M., and Batalla, R. J.: Bed load bias: Comparison of measurements obtained using two \(76 and 152  
1019 mm\) Helley-Smith samplers in a gravel bed river, \*Water Resour. Res.\*, 42, <https://doi.org/10.1029/2005WR004025>,  
1020 2006.](#)
- 1021 [Vericat, D., Wheaton, J. M., and Brasington, J.: Revisiting the Morphological Approach, in: \*Gravel-Bed Rivers\*, John  
1022 Wiley & Sons, Ltd, 121–158, <https://doi.org/10.1002/9781118971437.ch5>, 2017.](#)
- 1023 Wheaton, J. M.: Uncertainty in morphological sediment budgeting of rivers, phd, University of Southampton, 2008.
- 1024 Wheaton, J. M., Brasington, J., Darby, S. E., and Sear, D. A.: Accounting for uncertainty in DEMs from repeat  
1025 topographic surveys: improved sediment budgets, *Earth Surf. Process. Landf.*, 35, 136–156,  
1026 <https://doi.org/10.1002/esp.1886>, 2010.
- 1027 [Wilcock, P. R.: Entrainment, displacement and transport of tracer gravels, \*Earth Surf. Process. Landf.\*, 22, 1125–1138,  
1028 \[https://doi.org/10.1002/\\(SICI\\)1096-9837\\(199712\\)22:12<1125::AID-ESP811>3.0.CO;2-V\]\(https://doi.org/10.1002/\(SICI\)1096-9837\(199712\)22:12<1125::AID-ESP811>3.0.CO;2-V\), 1997.](#)

1029 [Wu, S., Feng, F., Zhu, J., Wu, C., and Zhang, G.: A Method for Determining Intrinsic Mode Function Number in](#)  
1030 [Variational Mode Decomposition and Its Application to Bearing Vibration Signal Processing, Shock Vib., 2020, 1–16,](#)  
1031 [https://doi.org/10.1155/2020/8304903, 2020.](https://doi.org/10.1155/2020/8304903)

1032

Formatted: Font: Not Bold

1033

1034

1035

Formatted: heading